JOURNAL OF GEOPHYSICAL RESEARCH, VOL. 101, NO. B2, PAGES 3311–3332, FEBRUARY 10, 1996

Effects of strongly variable viscosity on three-dimensional compressible convection in planetary mantles

Paul J. Tackley[1]

Seismological Laboratory, California Institute of Technology, Pasadena

Abstract. A systematic investigation into the effects of temperature dependent viscosity on three-dimensional compressible mantle convection has been performed by means of numerical simulations in Cartesian geometry using a finite volume multigrid code, with a factor of 1000-2500 viscosity variation, Rayleigh numbers ranging from 10^5-10^7, and stress-free upper and lower boundaries. Considerable differences in model behavior are found depending on the details of rheology, heating mode, compressibility, and boundary conditions. Parameter choices were guided by realistic Earth models. In Boussinesq, basally heated cases with viscosity solely dependent on temperature and stress-free, isothermal boundaries, very long wavelength flows (~25,000 km, assuming the depth corresponds to mantle thickness) with cold plumes and hot upwelling sheets result, in contrast to the upwelling plumes and downwelling sheets found in small domains, illustrating the importance of simulating wide domains. The addition of depth dependence results in small cells and reverses the planform, causing hot plumes and cold sheets. The planform of temperature dependent viscosity convection is due predominantly to vertical variations in viscosity resulting from the temperature dependence. Compressibility, with associated depth-dependent properties, results in a tendency for broad upwelling plumes and narrow downwelling sheets, with large aspect ratio cells. Perhaps the greatest modulation effect occurs in internally heated compressible cases, in which the short-wavelength pattern of time-dependent cold plumes commonly observed in constant-viscosity calculations completely changes into a very long wavelength pattern of downwelling sheets (spaced up to 24,000 km apart) with time-dependent plumelike instabilities. These results are particularly interesting, since the basal heat flow in the Earth's mantle is usually thought to be very low, e.g., 5-20% of total. The effects of viscous dissipation and adiabatic heating play only a minor role in the overall heat budget for constant-viscosity cases, an observation which is not much affected by the Rayleigh number. However, viscous dissipation becomes important in the stiff upper boundary layer when viscosity is temperature dependent. This effect is caused by the very high stresses occurring in this stiff lid, typically 2 orders of magnitude higher than the stresses in the interior of the domain for the viscosity contrast modeled here. The temperature in the interior of convective cells is highly sensitive to the material properties, with temperature dependent viscosity and depth-dependent thermal conductivity strongly increasing the internal temperature, and depth-dependent viscosity strongly decreasing it. The sensitivity of the observed flow pattern to these various complexities clearly illustrates the importance of performing compressible, variable-viscosity mantle convection calculations with rheological and thermodynamic properties matching as closely as possible those of the Earth.

Introduction

Arguably the most important varying material property of mantle minerals is the extreme temperature dependence of the viscosity as well as its dependence on pressure and stress [*Weertman*, 1970; *Weertman and Weertman*, 1975; *Stocker and Ashby*, 1973; *Durham et al.*, 1979]. Viscosity is likely to vary by many orders of magnitude over the range of conditions encountered in the mantles of Earth or Venus, and thus, if we are to obtain a complete understanding of the mantle convective process, viscosity variations are an essential component in numerical models. In order to simultaneously obtain the range of features observed in planetary mantle convection, for example, linear slabs, cylindrical plumes, and toroidal motion, three-dimensionality (3-D) is also an essential ingredient. Indeed, two-dimensional (2-D) rolls become unstable to 3-D disturbances at a fairly low Rayleigh number, both with rigid [*Busse*, 1967; *Richter*, 1978; *Frick et al.*, 1983] and stress-free [*Travis et al.*, 1990a; *Christensen and Harder*, 1991] upper and lower boundaries. Although there has been much progress in 3-D modeling of mantle convection over the past decade, it has only recently become possible to

[1]Now at Department of Earth and Space Sciences, University of California, Los Angeles.

Paper number 95JB03211.
0148-0227/96/95JB-03211$05.00

include large viscosity variations in time-dependent, 3-D models with wide domains [*Tackley*, 1993; *Balachandar et al.*, 1995a,b]. The purpose of this present study is to further analyze and greatly extend the Boussinesq, basally heated results of *Tackley* [1993], focusing on the effects of compressibility, internal heating, depth dependence of the viscosity, and Rayleigh number, on mantle circulation with temperature dependent viscosity.

It is instructive to review our current understanding of 3-D mantle convection as it relates to this present study, starting with constant-viscosity fluids and progressing to variable-viscosity fluids. Both laboratory and numerical studies have been performed. Although laboratory experiments have played a useful role, they are limited in their applicability to the Earth by (amongst other things) the common use of rigid boundary conditions, since the mobility of plates on the Earth suggests that stress-free boundary conditions are more appropriate, although still far short of being a realistic boundary condition.

Constant Viscosity Studies

Boussinesq. The Boussinesq approximation [*Boussinesq*, 1903; *Rayleigh*, 1916], in which density is assumed constant except for weak variations with temperature which appear in the bouyancy term of the momentum equation, and (usually) material properties are assumed constant, has commonly been used in studies of mantle convection. Numerical simulations and laboratory experiments on Boussinesq fluids with constant material properties at moderate Rayleigh numbers (Ra) in rectangular Cartesian boxes have indicated that many different convective patterns are possible at a particular Ra, depending on the initial conditions, size of box, boundary conditions, and heating mode.

For basally heated convection between rigid upper and lower boundaries, laboratory experiments [*Whitehead and Parsons*, 1978] show that spoke patterns (i.e., upwelling and downwelling plumes interconnected at the boundaries by an irregular polygonal network of linear spokes) or bimodal patterns (i.e., orthogonal superimposed rolls) are possible over the Ra range 5×10^4 to 7.6×10^5, with square patterns being possible at the highest Ra. The stability of square and bimodal patterns were investigated numerically by *Frick et al.* [1983], who computed steady solutions in periodic boxes with rigid upper and lower boundaries for Ra up to 2.6×10^4, finding that squares were unstable over this parameter range, decaying into rolls or bimodal flow.

Free-slip upper and lower boundaries are arguably more relevant to the Earth. At $Ra=10^5$ and with free-slip boundaries, stable solutions include rolls, bimodal flow, up-squares (i.e., upwelling hot plumes surrounded by square patterns of downwelling cold sheets), down-squares (i.e., downwelling cold plumes surrounded by square patterns of upwelling hot sheets), and hexagons, as shown by the numerical models of *Travis et al.* [1990a]. The pattern obtained depends on details of domain aspect ratio, Ra and initial conditions. At much higher Ra, that is, greater than about 10^7, these simple patterns break down into a complex time-dependent flow characterized by disconnected upwelling and downwelling plumes emanating from irregular cellular ridge patterns at the upper and lower boundaries, as shown by the numerical experiments of *Malevsky and Yuen* [1993].

In these simple cases with constant material properties, identical upper and lower mechanical and thermal boundary conditions and no internal heating, patterns are symmetric with respect to upwellings and downwellings, with, for example, downwelling plumes (as found in down-squares or hexagons, for example) being equally as likely as upwelling plumes (as in up-squares or hexagons). This symmetry is, however, broken by (1) internal heating, (2) compressibility (with associated depth-dependent properties), (3) spherical geometry, and (4) temperature dependent viscosity. These effects will now be discussed.

Internal heating. It is thought that the mantle resembles to first order an internally heated fluid [*Schubert*, 1979], with core heat flow accounting for only 6-20% of the surface heat flow [*Davies*, 1988; *Sleep*, 1990; *Davies and Richards*, 1992; *Stacey*, 1992], secular cooling accounting for up to 30% [*Sharpe and Peltier*, 1978; *Schubert et al.*, 1980; *Stacey*, 1992; *Breuer and Spohn*, 1993], and the remainder due to the radioactive decay of elements ^{238}U, ^{232}Th, and ^{40}K in the mantle [*Turcotte and Schubert*, 1982; *Stacey*, 1992]. Laboratory experiments on internally heated plane layers with rigid boundary conditions [e.g., *Carrigan*, 1985 and references therein] have generally focused on the stability of hexagonal patterns, finding that up-hexagons (i.e., upwelling hot plumes surrounded by hexagonal cold sheets) are preferred at higher Ra. With free-slip boundaries, however, internally heated convection is characterized by isolated cold downwelling plumes amidst a diffuse hot upwelling flow. *Schubert et al.* [1993] obtained steady state, internally heated Boussinesq solutions at a Ra of 1.4×10^4 in both Cartesian and spherical geometries, finding that several solutions were possible. However, internally heated convection becomes time dependent at lower Ra than basally heated convection [*Schubert and Anderson*, 1985], and the resulting patterns are characterized by relatively closely spaced, transient cold plumes, with sheetlike interconnections at the upper boundary layer, and little or no long-lived coherent structure, as illustrated by *Houseman* [1988] at $Ra=5.9\times10^5$ and *Parmentier et al.* [1994] at Ra up to 3×10^7. Convection heated partly from within and partly from below has been investigated by *Houseman* [1988], *Weinstein and Olson* [1990], and *Travis et al.* [1990b], who find that as the fraction of internal heating is decreased, downwellings become more sheetlike and interconnected.

Compressibility. The studies discussed above all assume the Boussinesq limit. Compressibility, which implies depth dependence of material properties as well as additional terms in the equations, has been included in the Cartesian, basally heated calculations of *Balachandar and Yuen* [1992] and *Balachandar et al.* [1993]. They find that compressibility breaks the symmetry between upwellings and downwellings, resulting in very broad, strong hot upwelling plumes surrounded by interconnected narrow cold downwelling sheets.

Spherical geometry. Spherical geometry also breaks the symmetry between upwellings and downwellings, resulting in a strong preference for plumelike upwellings and sheetlike downwellings. Early results [*Young*, 1974; *Machetel et al.*, 1986] were at only mildly supercritical Ra. Strongly supercritical Boussinesq, steady state solutions with tetrahedral and cubic arrangements of plumes were obtained at Ra up to 7×10^4 by *Bercovici et al.* [1989a]. Compressible solutions at relatively high Rayleigh numbers [*Baumgardner*,

1985, 1988; *Glatzmaier*, 1988; *Bercovici et al.*, 1989b,c; *Glatzmaier et al.*, 1990; *Schubert*, 1992] confirm that the preferred form of convection is upwelling plumes and downwelling sheets, with the downwelling sheets becoming disconnected and plumelike as the degree of internal heating increases, as in the Cartesian models discussed earlier.

Other complexities that have been considered in 3-D constant-viscosity mantle convection include layering [*Olson*, 1984; *Cserepes et al.*, 1988; *Glatzmaier and Schubert*, 1993], plates [*Cserepes and Christensen*, 1990; *Gable et al.*,1991], and phase transitions [*Tackley et al.*, 1993, 1994; *Honda et al.*, 1993; *Yuen et al.*, 1994]. These, while not considered in this present study, may form the focus of future research.

Variable Viscosity Studies

By far the largest approximation in all the above calculations is the assumption of viscosity which is constant, or only depth dependent. The viscosity of the Earth's mantle is known to be very strongly temperature dependent, which is certain to affect the pattern of convection. Thus it is essential to include such rheology in laboratory or numerical studies.

The main results established by laboratory experiments (with rigid boundaries) are as follows.

1. If the Ra is defined using the viscosity for the average of top and bottom boundary temperatures, the dependence of Nusselt number (Nu) on Ra is not greatly affected by viscosity contrast. This was shown at Ra=10^5 and viscosity contrasts of up to 300 by *Booker* [1976], and later corroborated by *Richter et al.* [1983] and *Giannandrea and Christensen* [1993].

2. Stable solutions include rolls, bimodal, hexagons, squares, and spokes. The stability diagram of these as a function of Ra and viscosity contrast was mapped out by *White* [1988] for Ra up to $6.3\text{x}10^4$ and viscosity contrasts up to 1000. Increasing temperature dependence of viscosity lowers the Ra at which patterns become unstable to spoke-pattern flow, to about $2.5\text{x}10^4$ for a viscosity variation of 1000. Squares and hexagons are stable at lower Ra, and rolls or bimodal flow are stable at lower viscosity contrasts.

Numerical work has focused mainly on steady state solutions in small boxes, and much of it has concentrated on reproducing laboratory experiments rather than modeling the Earth. The experimental observation of *Booker* [1976] (i.e., that rolls are stable at low viscosity contrasts, with squares at high viscosity contrasts) was verified numerically by *Busse and Frick* [1985] in a square box with linear dependence of viscosity on temperature and rigid upper and lower boundaries. The more realistic case of stress-free boundaries was modeled by *Ogawa et al.* [1991], who obtained steady state solutions at low Ra and viscosity contrasts of up to 10^5 in a highly restrictive 0.5x1.7x1 box. The stagnant lid regime, characterized by upwelling plumes and downwelling sheets beneath a stagnant lid, was obtained at high viscosity contrasts, whereas the whole-mantle regime, in which the surface boundary layer participates in the flow, was obtained at lower contrasts. The latter regime is characterized by upwelling and downwelling plumes with sheetlike extensions. Steady state solutions in small boxes (aspect ratio up to 1.5) with various boundary conditions, Ra up to 10^5 and viscosity contrasts of up to 1000, were obtained by *Christensen and Harder* [1991], who mapped the domains of stability for squares (which are unstable at low viscosity contrasts) and rolls (which are unstable at high viscosity contrasts and low Ra). For their experimental conditions, temperature dependent viscosity favors upwelling plumes and downwelling sheets. For larger domains and rigid boundaries, additional patterns were obtained, including up-hexagons and triangles, and, in a 4x4x1 box with a viscosity contrast of 30, they obtained spoke-pattern flow. However, the pattern is changed completely to a long-wavelength pattern consisting of upwelling sheets and a downwelling plume simply by changing the upper boundary condition to stress free, as demonstrated by *Weinstein and Christensen* [1991]. This result was confirmed experimentally by *Giannandrea and Christensen* [1993], although they also found that at much higher viscosity contrasts (above ~1000) a stagnant lid develops, and the pattern becomes similar to that obtained with a rigid lid. The fundamental effects of boundary conditions and box size were further demonstrated by *Tackley* [1993], who presented solutions in an 8x8x1 periodic box with Ra=10^5 and viscosity contrast of 1000. With rigid boundaries, small aspect ratio spoke-pattern flow was obtained, but with stress-free boundaries, a large aspect ratio down-square pattern (i.e., with a downwelling cold plume and upwelling sheets) was obtained.

All of the above solutions are basally heated and in the Boussinesq limit, whereas it is well established that the Earth's mantle is substantially internally heated, and that the effects of compressibility play a significant role. Clearly, it is necessary to establish how these results are affected by such complications, as well as depth dependence of viscosity and higher Ra. In this paper we start from the results of *Tackley* [1993] and systematically investigate the effect of these additional complexities.

Model, Method, and Parameters

Equations

As is standard in studies of mantle convection, we make the infinite-Prandtl-number approximation, neglecting inertial terms in the momentum equation, which is valid because the Prandtl number for the mantle is of the order of 10^{24}, and we also make the anelastic approximation, which is valid because the sound velocity is much faster than convective velocities. For computational convenience we make the anelastic-liquid approximation, discussed by *Jarvis and McKenzie* [1980], in which the influence of dynamic pressure on temperature is neglected. Since this term is of the order of 10^{-2}, this approximation is not expected to have much impact on the results. The equations are nondimensionalized to the depth of the mantle (D), thermal diffusion timescale (D^2/κ, where κ is thermal diffusivity) and superadiabatic temperature drop, ΔT_{sa}. Other nondimensionalizations, for example, velocity (κ/D) and stress ($\eta\kappa/D^2$), follow from these.

The equations are those of continuity,

$$\nabla \bullet (\bar{\rho}\mathbf{v}) = 0 \tag{1}$$

conservation of momentum,

$$\nabla \bullet \tilde{\tau} - \nabla p = Ra\, \overline{\alpha\rho} T \hat{\mathbf{z}} \qquad \tau_{ij} = \eta(v_{i,j} + v_{j,i} - \tfrac{2}{3} v_{k,k}\delta_{ij}) \tag{2}$$

and conservation of energy,

$$\bar{\rho}\bar{C}_p \frac{DT}{Dt} = -Di_s \overline{\alpha\rho} T v_z + \nabla \bullet (\bar{k}\nabla T) + \bar{\rho}\bar{H} + \frac{Di_s}{Ra}\tau_{ij} v_{i,j} \tag{3}$$

where the surface dissipation number Dis is given by

$$Di_s = \frac{\alpha_s g D}{C_{ps}} \quad (4)$$

v, p, T, τ, and η and D are velocity, dynamic pressure, absolute temperature, deviatoric stress, dynamic viscosity, and depth of mantle, respectively, $\mathbf{z}$ is a unit vector in the vertical direction, and the overbarred quantities ρ, α, C_p, κ, and k ($=\rho C_p \kappa$) are depth-dependent reference state parameters density, thermal expansivity, heat capacity, thermal diffusivity, and thermal conductivity, respectively. The subscript s indicates the surface value, and the vertical coordinate z runs from 0 at the base to 1 at the surface. The Boussinesq approximation is recovered by setting Di=0 and all depth-dependent properties to 1.

The definition of Ra for a system with variable coefficients, in particular viscosity, is somewhat arbitrary. We choose a definition based on the surface values of reference state variables, and the viscosity for the value of the reference adiabat at the surface, T_{as}, representing an "upper mantle" viscosity. Since thermodynamic properties are much better constrained in the shallow mantle than in the deep mantle, this "surface" Rayleigh number, Ra_s is also better constrained than any of the other Ra definitions. For Boussinesq cases the reference adiabat is T=0.5, and with viscosity dependent solely on temperature, the Ra thus defined is identical to $Ra_{1/2}$ used by many authors [e.g., *Booker*, 1976]. The Ra based on the viscosity at the surface boundary condition rather than adiabat [e.g., *Ogawa et al.*, 1991; *Hansen et al.*, 1993] would be approximately 2 orders of magnitude lower. In cases with depth-dependent viscosity, an alternative choice would be to use the viscosity on the reference adiabat at middepth: this Ra is approximately an order of magnitude lower than the stated values. A volume-averaged Ra [e.g., *Glatzmaier*, 1988] is awkward to use, since $<\eta>$ is an output quantity, and it is desirable to use a definition of Ra that includes only input parameters.

Thus

$$Ra_s = \frac{\rho_s g \alpha_s \Delta T_{sa} D^3}{\eta(T_{as},0)\kappa_s} \quad (5)$$

where g is the gravitational acceleration and the other quantities have already been defined. It is important to note the distinction between this Ra, which is based on the whole-mantle depth (D) and superadiabatic temperature drop ΔT_{sa}, and the "local" Ra [*Howard*, 1966] used later in this paper to develop various scaling relationships. The latter is based on the thickness of and temperature drop over an individual boundary layer, and is used to predict when that boundary layer will become convectively unstable.

Viscosity

In keeping with the Earth's mantle, we use an Arrhenius law [*Weertman*, 1970] to describe the variation of viscosity with temperature, which gives more rapid viscosity variations at low temperatures than at high temperatures. A linearized exp(-aT) law has commonly been used in numerical studies for convenience, but this is quite unrealistic.

Unfortunately, the viscosity variations that can be modeled are limited by the convergence of the numerical method, and thus the viscosity law that is used is a compromise between the ideal law and that which is numerically tractible. The following compromises are made. (1) We use a nondimensional activation energy of 13.8155 (nondimensionalized to $R\Delta T_{sa}$, where R is the gas constant) that is lower than measured values. For example, the value of 540 kJ mol^{-1} for dry olivine measured by *Karato and Wu* [1993] corresponds to 26.0 nondimensional units. (2) The temperature that appears in the denominator of the Arrhenius law is offset from the absolute nondimensional model temperature, in order to avoid the extremely large viscosities that would otherwise occur in the upper thermal boundary layer. (3) The depth dependence of viscosity, when included, is specified as an exponential dependence on depth, rather than an activation volume. If an activation volume were used, it would have an effect similar to a large activation energy in the deep mantle, resulting in very large viscosity variations [*van Keken et al.*, 1994], which would cause numerical difficulties.

The resulting viscosity law is as follows:

$$\eta(T,z) = A_0 \exp[-z \ln \Delta\eta_z] \exp\left[\frac{13.8155}{T+T_{off}}\right] \quad (6)$$

where A_0 is calculated such that $\eta(T_{as},1) = 1.0$, where T_{as} is the surface temperature value of the reference adiabat; $\Delta\eta_z$ is the fractional variation of viscosity between the upper and lower boundaries due to pressure dependence, and is taken to be 1 or 100. T_{off} is the temperature offset added to the nondimensional temperature to reduce the viscosity variation across the upper boundary, and is taken to be 1.0 for Boussinesq cases (in which the surface temperature boundary condition is 0) and 0.88 for compressible cases (in which the surface temperature boundary condition is 0.12).

The resulting viscosity variation due to temperature is a factor of 1000 for Boussinesq cases, independent of depth. For compressible cases, the variation is a factor of ~500 near the surface, ~2000 near the core-mantle boundary (CMB), and ~2500 between the upper boundary condition and lower boundary condition. This variation would be reduced if non-Newtonian rheology, which may be important in some regions of the mantle [*Karato and Wu*, 1993], were included, as discussed later.

Reference State

Over the depth (pressure) range of the mantle, density and thermodynamic quantities vary significantly. Here we use a simple thermodynamic model to calculate $\rho(z)$ and $\alpha(z)$. Heat capacity C_p is assumed constant, as may be approximately true in the Earth's mantle, and thermal conductivity $k(z)$ is assumed to vary with the fourth power of density, giving an increase consistent with experiments [*Osako and Ito*, 1991] and theory [*Anderson*, 1987].

The magnitude of temperature and density stratification is controlled by dissipation number Di and compressibility number K respectively:

$$Di = \frac{\alpha g D}{c_p} \qquad K = \frac{\alpha g D}{\gamma c_p} = \frac{Di}{\gamma} \quad (7)$$

$$\frac{\partial \overline{T}}{\partial z} = -Di\overline{T} = -Di_s \frac{\overline{\alpha}}{\overline{c}_p}\overline{T} \qquad \frac{\partial \overline{\rho}}{\partial z} = -K\overline{\rho} = K_0 \frac{\overline{\alpha}}{\overline{c}_p}\left(\frac{\gamma_0}{\gamma}\right)\overline{\rho} \quad (8)$$

where g is the Gruneisen parameter and the other symbols were defined earlier. To complete the equations, variations of g and α must be specified. As is often assumed, we take $\gamma\rho = \text{const}$ [*Duffy and Ahrens*, 1993] and relate α to compression using the derivation of *Anderson et al.* [1992], which gives a very similar result to *Chopelas and Boehler* [1992]:

$$\left(\frac{\partial \ln \alpha}{\partial \ln \rho}\right)_T = \delta_T = \delta_{T0}\left(\frac{\rho_0}{\rho}\right)^n \tag{9}$$

giving

$$\alpha = \alpha_0 \exp\left[-\frac{\delta_{T0}}{n}\left(1-\left(\frac{\rho_0}{\rho}\right)^n\right)\right] \tag{10}$$

where δ_{T0} = 6.0, n=1.4. For the Boussinesq cases, Di=K=0, giving constant coefficients.

Thus, in order to construct the nondimensional reference state, the following surface quantities must be specified: Di_s, T_{as}, K_s, and γ_s. This leads to depth variations of ρ, α and κ, which are all assumed to be 1.0 at the surface. The resulting volume-averaged value of Di is 0.44, comparable to that thought to be appropriate for the Earth. Note that the surface Di, as quoted by other authors [e.g., *Balachandar and Yuen*, 1992] should be much higher. The adiabatic temperature increase for a reference adiabat is also calculated, although this is not used during the calculation, since absolute nondimensional temperatures are used.

These input parameters were chosen to give good fits to recent thermodynamic analyses of the lower mantle [*Chopelas and Boehler*, 1992; *Anderson et al.*, 1992; *Duffy and Ahrens*, 1993] and are listed in Table 1. Since density jumps associated with phase transitions are not included, the density increase over the entire mantle is not as large as in Earth models such as PREM [*Dziewonski and Anderson*, 1981]. Table 1 also lists typical dimensional values. These dimensional values are not used during the calculation, but are given to allow quantitative comparison of the results with observations. The resulting depth variation of density, temperature, thermal expansivity, thermal conductivity, and thermal diffusivity is illustrated in Figure 1, and Table 1 lists basal values of these and other quantities.

Since the definition of Rayleigh number is extremely ambiguous when coefficients are varying with temperature and depth, as discussed earlier, a better guide to how close convection is to the Earth-like regime can be obtained by considering observational measures such as heat flux and convective velocity. Thus Table 1 lists typical conversions between nondimensional and dimensional values for these quantities. The Earth's total heat flux of 87 mW m^{-2} [*Pollack et al.*, 1993] corresponds to a nondimensional flux of 35 units; however, this includes heat loss from radioactive elements in the crust; more appropriate is the mantle heat flux of 60-70 mW m^{-2} [*Stacey*, 1992; *Pollack et al.*, 1993], which corresponds to 24-28 nondimensional units. A velocity of 1 cm/year corresponds to 1500 nondimensional units.

The radioactive heating rate in carbonaceous chondrites, which are usually thought to be representative of mantle material [*Stacey*, 1992] is 5.2×10^{-12} W kg^{-1}, corresponding to 23.2 nondimensional units. In a Cartesian box, this would lead to a surface heat flux of ~70 mW m^{-2}, similar to the entire mantle heat flux given above. However, this is misleading, since in spherical geometry the ratio of mantle mass to

Table 1. Thermodynamic Parameters

Parameter	Symbol	Value	Units	Nondimensional Value
	Input Surface Parameters			
Dissipation number	Di_s	-	-	1.2
Compressibility number	Co_s	-	-	1.1
Gruneisen parameter	γ_s	-	-	1.091
Reference adiabat	T_{as}	1600	K	0.64
Boundary temperature	T_s	300	K	0.12
	Nondimensionalization			
Superadiabatic temperature	ΔT_{sa}	2500	K	1.0
Density: surface	ρ_s	4000	kg m^{-3}	1.0
Expansivity: surface	α_s	5.0×10^{-5}	K^{-1}	1.0
Conductivity: surface	k_s	3.0	W m^{-1} K^{-1}	1.0
Heat capacity	C_p	1200	J kg^{-1} K^{-1}	1.0
Depth of mantle	D	2890	km	1.0
	Derived Quantities			
Mean dissipation	$\langle Di \rangle$	-	-	0.441
Gruneisen parameter: CMB	γ_c	-	-	0.775
Adiabatic T rise	ΔT_a	900	K	0.36
Temperature: CMB	T_c	3700	K	1.48
Density: CMB	ρ_c	5600	kg m^{-3}	1.4
Expansivity: CMB	α_c	1.0×10^{-5}	K^{-1}	0.20
Conductivity: CMB	k_c	11.8	W m^{-1} K^{-1}	3.92
Velocity	v	1	cm yr^{-1}	1465
Time	t	423	Gyr	1.0
Heat flux	F	2.5	mW m^{-2}	1.0
Conductive heat flux	F_{cond}	7.5	mW m^{-2}	3.02
Internal heating rate	H	2.245×10^{-13}	W kg^{-1}	1.0
Chondritic heating rate	H_{chond}	5.2×10^{-12}	W kg^{-1}	23.2

CMB, core-mantle boundary.

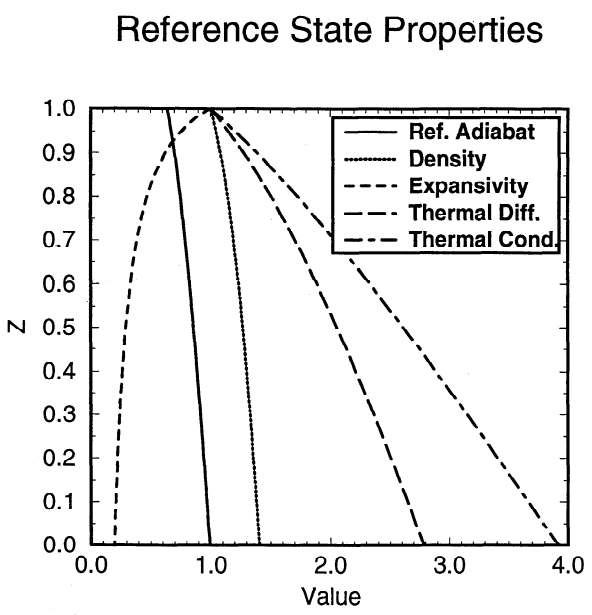

Figure 1. Variation of nondimensional reference-state thermodynamic parameters of density, temperature, thermal expansivity, thermal diffusivity, and thermal conductivity. For reference dimensional values, see Table 1.

surface area is much lower than in Cartesian geometry, and thus this chondritic heating rate would account for only ~40 mW m^{-2}, approximately 57-67% of the mantle heat flux. Thus, when performing numerical experiments in Cartesian geometry, it is appropriate to consider a heating rate that has been reduced according to this ratio, in order to give the correct surface heat flux. This reduced chondritic heating rate is 13.5 nondimensional units. However, it may also be appropriate to increase the internal heating rate to take account of the slow secular cooling of the mantle, which is not included in the present statistically steady state calculations, and resembles internal heating both mathematically (in the energy equation) and physically (in its effect on convection) [*Weinstein and Olson*, 1990].

Due to the increase of thermal conductivity and density with depth, the heat flux that would be conducted across the mantle in the absence of convection has a nondimensional value of 2.5, when the nondimensionalization is based on surface values of thermodynamic parameters. Thus the nondimensional heat flux is 2.5 times higher than the Nusselt number, when the latter is defined as the ratio of actual heat flux to the conductive heat flux. Indeed, if the increase of thermal conductivity given by *Osako and Ito* [1991] is correct, the Nusselt number of the Earth is in the range 10-13, much lower than commonly quoted values. For Boussinesq cases, Nusselt number is identical to heat flux.

Numerical Method

The exact details of the numerical method and its benchmarking are described elsewhere [*Tackley*, 1994] and are only briefly summarized here. The instantaneous velocity and pressure fields given by (1)-(3) are calculated by a finite difference (control volume) multigrid technique. Primitive variables (three components of velocity, and pressure) are defined on a staggered three-dimensional Cartesian grid, with vertical grid refinement in the upper and lower boundary layers. Use of a staggered grid apparently gives similar accuracy to a nonstaggered grid with twice the number of points in each direction [*Brandt*, 1982]. An iterative sweep consists of relaxing each equation in turn over the entire domain, and is similar, although not identical to, the SIMPLER method of *Patankar* [1980]. This iteration scheme is extremely robust, converging for almost any viscosity contrast. In addition, because the finite volume scheme is based on balancing surface stresses on the sides of volume elements with body forces within them, volume-integrated quantities are preserved to machine accuracy. The scheme is incorporated into a standard multigrid V-cycle [*Brandt*, 1982; *Press et al.*, 1992], giving an execution time which scales in proportion to the total number of grid points. Timestepping (equation (4)) is performed explicitly, using the multidimensional positive-definite advection transport algorithm (MPDATA) of *Smolarkiewicz* [1984] for advection, and second-order finite differences for diffusion, viscous dissipation, and adiabatic heating or cooling. Steps of typically 0.5-0.9 the Courant condition are used. The method is well suited to parallel computers, and the presented results were obtained on the Intel Touchstone Delta at the California Institute of Technology and the Intel Paragons at San Diego Supercomputer Center and the University of Hiroshima, Japan. Benchmarks and accuracy are described in detail in Appendix B of *Tackley* [1994]; a few examples are given here. For the two-dimensional constant-viscosity benchmark at $Ra=10^5$ (case 1b of *Blankenbach et al.* [1989]), Nusselt number and rms velocity are within 1.75% of the "correct" result for 16x16 cells, and 0.25% for 32x32 cells. With a temperature-dependent viscosity variation of 1000 and $Ra_{1/2}=3.162\times10^5$ (case 2a of *Blankenbach et al.* [1989]), these quantities are within 3% for 32x32 cells. For the three-dimensional benchmark cases 1a (constant viscosity) and 2 (temperature-dependent viscosity) of *Busse et al.* [1994], these quantities are within 2.6% with 8x8x8 cells, 1% with 16x16x16 cells, and 0.13% with 32x32x32 cells.

Results

Overview

The cases presented constitute a systematic progression from the simplest case (Boussinesq, constant-viscosity, basal heating) to the most complex case (compressible, with pressure- and temperature-dependent viscosity and internal heating), allowing the influence of each individual complexity to be clearly identified and understood.

The 27 cases presented are listed in Tables 2, 3 and 4, and are divided into three groups: Boussinesq with basal heating (Table 2, cases B1-B10), compressible with basal heating (Table 3, cases C1-C9), and compressible with internal heating (Table 4, cases I1-I8). Although the degree of basal heating for the Earth is probably in the range 6-20%, as discussed earlier, it is instructive to consider the limiting cases of completely basal and completely internal heating, in order to obtain a thorough understanding of the underlying fluid dynamics. Each group contains cases in which viscosity is constant, depth dependent, temperature dependent, and temperature and depth dependent, as well as cases with different Ra.

In all cases the upper boundary is impermeable, stress free, and isothermal. The lower boundary is impermeable and stress

Table 2. Simulation Characteristics for Boussinesq, Basally Heated Cases

Case	Ra_s	Viscosity	a bc	nh	nz	Start	Time	Nu	V_{rms}	$<T>$
B1	10^5	const	8 P	128	32	rand	0.437	9.05	196	0.486
B2	10^5	T	8 P	128	32	rand	0.629	6.22	192	0.629
B3	10^5	T	8 R	128	16r	rand	0.422	5.87	197	0.643
B4	10^5	T	4 R	64	16r	rand	0.898	5.95	187	0.636
B5	10^5	Z	4 R	64	16r	rand	2.164	3.58	40.1	0.338
B6	10^5	T+Z	4 R	64	16r	rand	1.86	3.30	28.8	0.434
B7	10^6	T	4 R	128	32r	B4	0.0484	12.6	791	0.685
B8	10^6	T+Z	4 R	128	32r	rand	0.166	6.75	99.7	0.408
B9	10^5	T[a]	8 P	128	16r	RSC	0.594	5.51	188	0.676
B10	10^5	T[b]	8 P	128	16r	RSC	0.314	11.8	300	0.486

"Ra" is $Ra_{1/2}$ as discussed in the text. For viscosity, T indicates temperature dependence and Z indicates Z dependence, with parameters as dicussed in the text. The "a" refers to aspect ratio, and side boundary conditions (bc) are periodic (P) or reflecting (R). The nh and nz are the number of horizontal and vertical grid cells, respectively, with an r indicating vertical grid refinement in the boundary layers. Here, "rand" indicates random start conditions, and RSC denotes case 2 of *Tackley* [1993] with $\eta(T)$ and rigid boundaries, which has a very small cell spoke pattern with upwelling plumes and downwelling sheets.

[a]Only vertical viscosity variations (see text for details).

[b]Mainly horizontal viscosity variations (see text for details).

free, and either isothermal (basally heated cases B1-10 and C1-9) or insulating (internally heated cases I1-8). Side boundaries are reflecting, except for cases B1, B2, B9, B10, and C9, in which they are periodic, as in *Tackley* [1993]. The computational domain consists of a 4x4x1 Cartesian box (i.e., 4 times wider than it is deep) except for cases B1-B3, which use an 8x8x1 box, and case C9, which uses a 16x16x1 box. The number of grid cells in the horizontal directions (nh) and vertical directions (nz) are listed in Table 2, where an "r" denotes (smoothly varying) vertical grid refinement in the boundary layers, by a factor of approximately 3. For example, a grid of nh=128, nz=32r in an aspect ratio 4 box gives a horizontal grid spacing of 90 km and a vertical grid spacing ranging from 36 km near to boundaries to 103 km near middepth, when dimensionalized to the mantle depth of 2900 km. Vertical grid refinement results in greatly improved accuracy compared to results with constant grid spacing, as shown by the benchmark tests in Appendix B of Tackley [1994]. Note that "grid spacing" is not synonymous with "resolution," since it is necessary to have at least two to three grid points across a convective feature in order to resolve it.

Starting conditions and run durations (one nondimensional time unit ≈ 423 Gyr) are also listed in Tables 2-4. Cases were started either from the final frame of a previous case, or from a random initial state consisting of an isothermal interior (T=0.5 for Boussinesq or the reference adiabat for compressible cases), error-function boundary layers at top and bottom, and small random (white noise) perturbations of amplitude 0.05. After initial transients, the flow patterns were generally found to evolve very slowly but steadily, requiring large integration times (up to nondimensional 2.1, or 10,000-19,000 time steps) to ensure solutions had overcome their transient nature and basal and surface heat fluxes were in good agreement. Mean temperature $<T>$, surface heat flux (equal to Nusselt number in the Boussinesq cases), and average (rms) velocity are also listed. Many cases are time dependent, and thus these values fluctuate somewhat; however, the fluctuations are not large, and the given values are representative of the system.

Studies of internally heated convection have typically used a temperature nondimensionalization based on the conductive heat flux, i.e., $\Delta T_{ref}=(HD^2)/\kappa$, where H is internal heating rate [e.g., *Parmentier et al.*, 1994]. This results in very low nondimensional temperatures when convection is strongly supercritical. However, when temperature dependent viscosity is included, it is important for nondimensional temperatures to be similar to those obtained in the basally heated results, so that similar viscosities are obtained. Thus the approach taken here is to use the same temperature scale in the internally heated cases as in the basally heated cases, and to choose the internal heating rate for a particular Ra_T in order to obtain the same surface heat flux, and thus similar nondimensional temperature differences, as in an equivalent basally heated case. This is simple, since in equilibrium the surface heat flux F is related to internal heating rate H by

$$F=H<\rho> \quad (11)$$

Table 3. Simulation Characteristics for Compressible, Basally Heated Cases

Case	Ra_s	a bc	Viscosity	nh	nz	Start	Time	F	V_{rms}	$<T>$
C1	10^6	4 R	const	64	32r	rand	1.1375	21.4	482	1.047
C2	10^6	4 R	Z	64	32r	rand	0.7022	12.1	149	0.808
C3	10^6	4 R	T	128	32r	C1	0.0450	13.7	662	1.148
C4	10^6	4 R	T+Z	128	32r	rand	0.0906	12.7	241	1.000
C5	10^5	4 R	T+Z	64	16r	rand	1.4576	6.55	45.7	1.001
C6	10^7	4 R	T+Z	128	64r	rand	0.041	25.5	1003	0.962
C7	10^7	4 R	Z	128	32r	C2	0.0529	22.2	587	0.771
C8	10^5	4 R	const	64	16r	rand	0.6503	10.7	122	1.056
C9	10^6	16 P	const	256	16r	rand	0.5993	21.4	490	1.029

Columns have the same meaning as in Table 2, except that Ra_s refers to the surface "adiabat" Rayleigh number (see equation (5)), and heat flux F replaces Nu.

Table 4. Simulation Characteristics for Internally Heated, Compressible Cases

Case	Ra_s	H	Viscosity	nh	nz	Start	Time	F	V_{rms}	$<T>$
I1	10^6	16	const	128	32r	rand	0.0631	20.2	181	1.05
I2	10^6	10	Z	128	32r	I1	0.253	12.6	106	0.852
I3	10^6	10	T	128	32r	I1	0.0386	12.5	379	1.204
I4	10^6	10	T+Z	128	32r	I1	0.3350	12.3	211	1.132
I5	10^5	8	const	64	16r	rand	0.2774	9.94	70.1	1.060
I6	10^5	5	T+Z	64	16r	I5	1.082	6.29	35.1	0.964
I7	10^7	32	const	256	64r	rand	0.0181	40.2	651	1.119
I8	10^7	20	T+Z	256	64r	rand	0.028	25.0	538	1.156

All cases are in a 4x4x1 box with reflecting side boundaries. Columns have same meaning as in Table 2, with the addition of H, the internal heating rate.

where $<\rho>$ is the volume-averaged nondimensional density. For example, the internal heating rates for I1-I4 have been chosen to give similar surface heat flows to cases C1-C4, respectively. As discussed later, the resulting temperature drops and hence viscosity contrasts over the upper boundary layer are similar.

Boussinesq Cases

The 10 Boussinesq cases presented are listed in Table 2 and illustrated in Figure 2. All cases are entirely heated from below and have different viscosity laws, different aspect ratios (8 or 4), and horizontal boundary conditions. Cases B1 and B2 are the same as cases 1 and 3, respectively, of Tackley [1993], and are included here for comparison with the new results. Case B1 has constant viscosity, B2-B4 have temperature dependent viscosity and different boundary conditions and aspect ratios, B7-B8 are as B4 and B6 except at a higher Ra of 10^6, and B9 and B10 are discussed in a later section. A $Ra_{1/2}$ of 10^5 is 2 orders of magnitude lower than that thought to be appropriate for the Earth's mantle, but similar to that used in previous numerical and laboratory studies, thereby allowing direct comparisons to be made.

In the constant viscosity case (case B1, Figure 2a) there is a rough symmetry between upwellings and downwellings, which both start off as sheets, decaying into plumes as they ascend or descend, respectively. The downwellings exhibit greater connectivity, reflected in $<T>$ (see Table 2) being slightly lower than 0.5; however, this is just by chance, since the equations are symmetric with respect to the vertical coordinate in this case. In small aspect ratio boxes, stable patterns at this Rayleigh number include 2-D rolls, bimodal flow, and square or hexagonal cells, depending on the box dimensions and initial conditions [*Travis et al.*, 1990a]. The weakly time-dependent pattern obtained lies somewhere between these extremes, also containing characteristics of the spoke pattern.

Temperature dependent viscosity. When temperature dependent viscosity is added, the downwellings merge to form one huge quasi-cylindrical downwelling, resulting in a single square cell filling the entire computational domain. Upwelling sheets extend all the way from the base to the surface. Although the overall pattern remained very stable throughout the remainder of the calculation, the exact details of upwellings and downwellings were highly time dependent. Thus two scales of flow are exhibited: the broad-scale flow which is very stable, and small-scale flow which is highly time dependent. In order to test the robustness of this solution to initial conditions, an additional calculation was performed, starting from the final state of a case with a rigid boundary (case 2 of *Tackley* [1993]). After a nondimensional time of ~0.1, a single square cell was again formed.

Boundary conditions and aspect ratio. In order to test the effect of horizontal boundary conditions, two additional simulations were performed using reflecting rather than periodic sides. In case B3, which has the same aspect ratio as B2, upwelling sheets are also obtained, with a similar aspect ratio to case B2, except with hexagonal rather than square cells. The pattern obtained in case B4, which has half the aspect ratio of case B2, is (once symmetry has been considered) identical to that of case B2, i.e., a square cell with periodicity of 8. In a periodic domain, the maximum possible wavelength of the flow pattern is equal to the width of the domain, but with reflecting sidewalls, the maximum possible wavelength is double the width of the domain. Thus the same flow pattern can be obtained in a 4x4x1 reflecting box (case B4) as in an 8x8x1 periodic box (case B2). Since it is computationally much more efficient to use a 4x4x1 box, the remainder of the reported simulations use the 4x4x1 reflecting box. It is interesting to note that case B3 could have formed a square cell with a periodicity of 16, but instead chose a pattern with similar aspect ratio to case B2, thus indicating that the preferred periodicity is closer to 8 than 16. The effect of limited domain size is further investigated in the compressible cases.

Depth-dependent viscosity. Case B5 has a viscosity which increases exponentially with depth by 2 orders of magnitude. The Nusselt number is extremely low, and the resulting pattern is almost one of two-dimensional rolls. This case has an extremely long integration time (2.16), but is still evolving very slowly. When the viscosity is dependent on temperature as well as depth (case B6), a short-wavelength, cellular pattern is observed, with upwelling plumes surrounded by interconnected downwelling sheets. Thus the addition of depth dependence has reversed the tendency to form large cells observed in cases where the viscosity is purely temperature dependent (e.g., case B4).

Rayleigh number. Cases B7 and B8 are identical to B4 and B6 but with Ra an order of magnitude higher, with a $Ra_{1/2}$ of 10^6 rather than 10^5. The overall patterns are very similar to the lower Ra cases, with B7 displaying narrower features and greater time dependence, and B8 displaying an even shorter-wavelength pattern than B6. Thus for these examples, Ra is not important in determining the basic pattern; it simply has a modulating effect on the detailed structure.

In these results, adding temperature dependent viscosity at a constant $Ra_{1/2}$ has reduced the Nusselt number by around 31%, from 9.05 (case B1) to 6.22 (case B2). This appears to

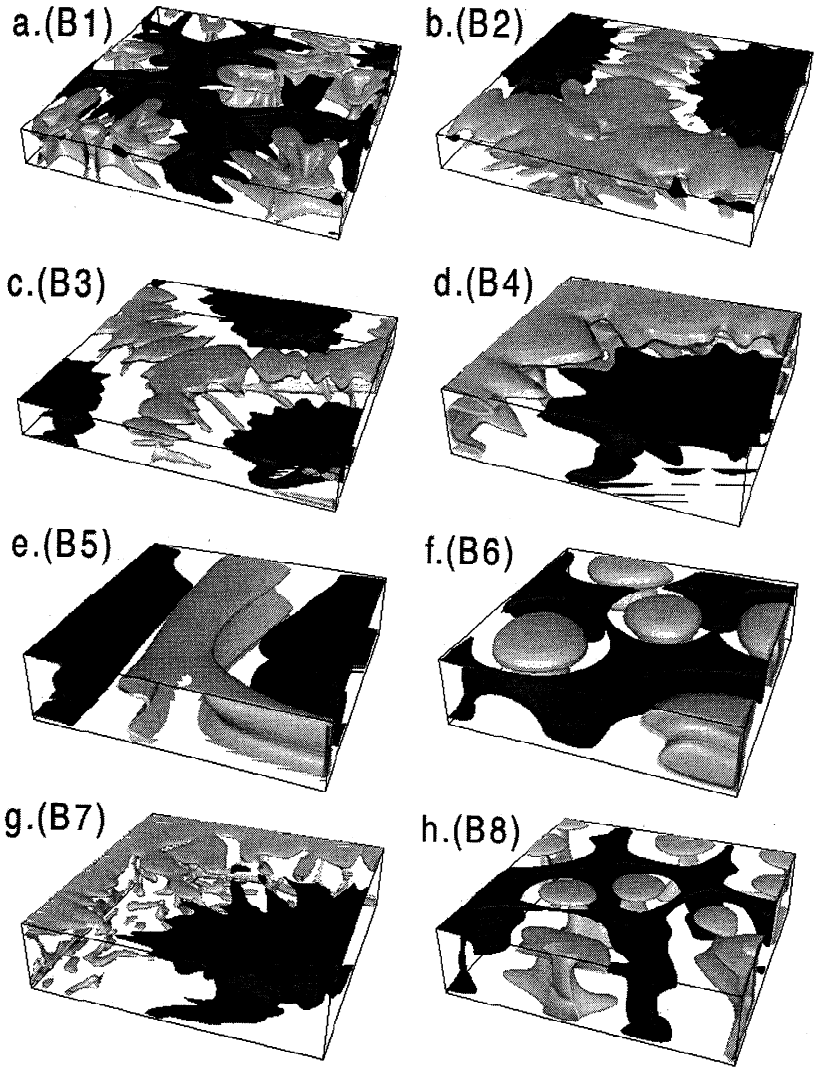

Figure 2. Convective patterns for Boussinesq, basally heated cases. Plotted are isosurfaces of residual temperature (i.e., temperature relative to horizontally averaged value). Light contours indicate upwellings, showing where the temperature is 0.1 hotter than the horizontal average; dark contours indicate downwellings, showing where the temperature is 0.1 colder than the horizontal average. (a) Constant viscosity, $Ra=10^5$ (B1); (b) $\eta(T)$, periodic sides, $Ra=10^5$ (B2); (c) $\eta(T)$, reflecting sides, $Ra=10^5$ (B3); (d) $\eta(T)$, aspect ratio 4, $Ra=10^5$ (B4), displaying the same solution as B2; (e) $\eta(Z)$, $Ra=10^5$ (B5); (f) $\eta(T,Z)$, $Ra=10^5$ (B6); (g) $\eta(T)$, $Ra=10^6$ (B7); and (h) $\eta(T,Z)$, $Ra=10^6$ (B8). For further details, see Table 2.

contradict the observation of *Booker* [1976], *Richter et al.* [1983], and *Giannandrea and Christensen* [1993], who find that Nusselt number does not change greatly with viscosity contrast when the upper boundary is rigid. The most important difference between the above laboratory experiments and the results presented here is probably this rigid upper boundary; when *Giannandrea and Christensen* [1993] used a free-slip upper boundary they found a decrease in Nusselt number with increasing viscosity contrast compatible with that observed here. A secondary difference may be that the viscosity law used here gives much greater viscosity variation for cold temperatures than for hot temperatures (a factor of 100 between $T=0.0$ and $T=0.5$, but only a factor of 10 between $T=1.0$ and $T=0.5$), whereas the viscosity law of the laboratory fluids gave a more equal distribution. The volume-averaged rms velocity is not significantly affected by temperature dependent viscosity.

Compressibility

Nine compressible, basally heated cases are presented, listed in Table 3, seven of which are illustrated in Figure 3. As discussed earlier, compressibility implies the depth dependence of thermal expansivity, thermal conductivity, and density, as well as the addition of viscous dissipation and adiabatic heating to the energy equation.

With constant viscosity (case C1), a single, square cell with a broad upwelling plume surrounded by time-dependent, downwelling sheets is observed. This result is similar to that obtained by *Balachandar and Yuen* [1992] in a 5x5x1 periodic box using a completely different numerical technique (a spectral method). When compared to case B1, in which both upwellings and downwellings start as sheets and decay into plumes, the effect of compressibility in breaking the symmetry between upwellings and downwellings becomes clear. Since

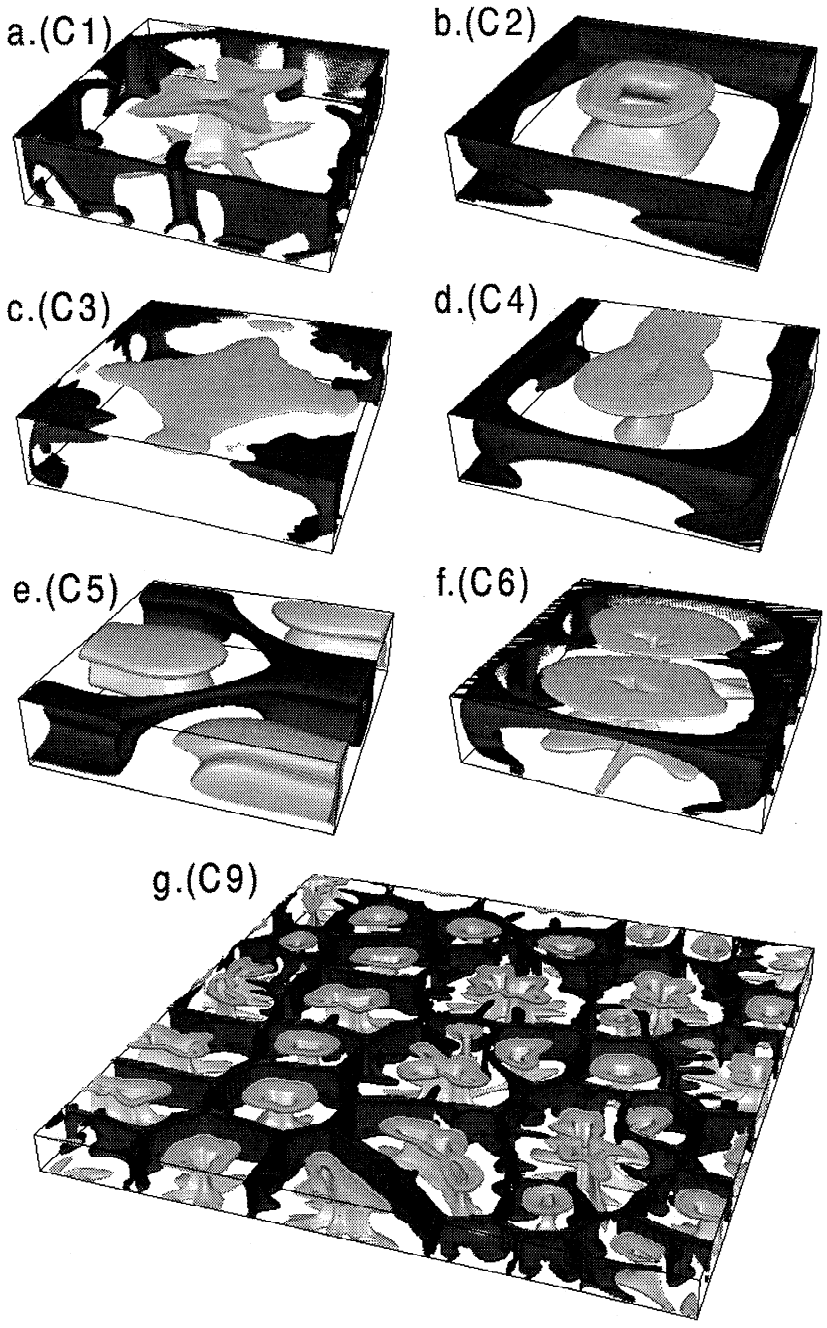

Figure 3. Convective patterns for compressible, basally heated cases. Isocontours show the same T values as for Figure 2. (a) constant viscosity, Ra=10^6 (C1); (b) $\eta(Z)$, Ra=10^6 (C2); (c) $\eta(T)$, Ra=10^6 (C3); (d) $\eta(T,Z)$, Ra=10^6 (C4); (e) $\eta(T,Z)$, Ra=10^5 (C5); (f) $\eta(T,Z)$, Ra=10^7 (C6); and (g) C9, same as C1 but in a 16x16x1 periodic box. Further details are given in Table 3.

the downwellings appear to follow the sides of the domain an obvious question is how much the box is constraining the solution. This question is addressed in case C9 (Figure 3g), which has the same parameters but in a much larger 16x16x1 periodic box. The basic nature of the solution is the same (broad upwelling plumes and narrow downwelling sheets), the difference being that the cells are slightly smaller and form an irregular polyhedral pattern rather than square cells.

When the viscosity is dependent on depth only (case C2), the central plume becomes much broader at its base, decreasing in thickness as it ascends. Both the upwelling plume and downwelling sheets are stabilized, resulting in a steady state solution at this Ra.

When the viscosity is dependent on temperature only (case C3), four cylindrical downwellings occur at the corners of the box. The interior of the convective cell has heated up greatly, so that the temperature contrast between the upwellings and downwellings is very small. However, the upwellings are indeed sheetlike, as with the equivalent Boussinesq case (B2). Thus the sheetlike nature of the upwellings with temperature dependent viscosity is not affected by compressibility.

The addition of depth dependence (case C4) to the temperature dependence, however, again results in a strong central plume. Although still broader at its base (as with C2), the temperature dependence has reduced the amount of broadening. Downwellings are linear in the shallow mantle, decaying into more cylindrical forms before they reach the base of the box. The elongation of the central plume, resulting in the formation of a 4x8 rectangular pattern, indicates a preference for larger cell size.

The effect of varying *Ra* is examined in cases C5 and C6, which have the same parameters as C4 but *Ra* an order of magnitude higher and lower, at 10^5 and 10^7, respectively. At the lower *Ra* (C5) the local *Ra* at the base of the box is subcritical, and penetrative convection occurs, with somewhat smaller cells. However, the convective vigor in this case is so low, that this pattern may be greatly influenced by starting conditions. This was confirmed by rerunning the case, starting from case C4; the long wavelength pattern of C4 was also a stable solution. At the higher *Ra* (case C6) an up-square is again formed, but the flow is highly time dependent. A preference for smaller cell size than case C4 is exhibited, suggesting that cell size may diminish at higher *Ra* for a fixed viscosity contrast.

Internal Heating

The eight internally heated, compressible cases are listed in Table 4 and plotted in Figure 4. With constant viscosity (case I1), a time dependent network of downwelling plumes interconnected at the surface by sheets is formed, similar to previous Boussinesq calculations [e.g., *Houseman*, 1988]. When depth dependence is added, however, these merge to form downwelling sheets, with a single square cell filling the box, although the small-scale structure suggests that a slightly shorter wavelength pattern would be preferred. Interestingly, a broad hot upwelling plume is observed in the center, even though there is no heat entering the base. This broad hot region is a passive feature.

When temperature dependent viscosity is added, the pattern changes greatly. A large-scale flow is set up, with a complex, highly time dependent region of downwelling near one edge of the box. Time dependent, transient ridges emanate radially

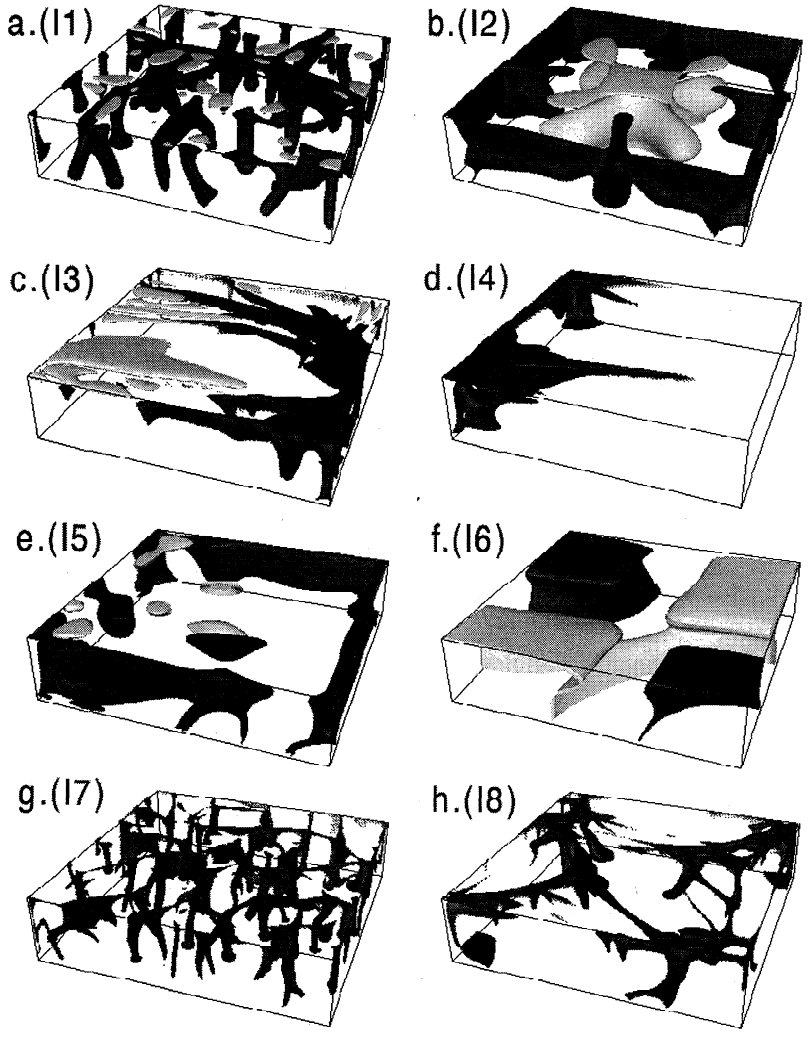

Figure 4. Convective patterns for compressible, internally heated cases. Isocontours show the same T values as for Figure 2. (a) Constant viscosity, $Ra=10^6$ (I1); (b) $\eta(Z)$, $Ra=10^6$ (I2); (c) $\eta(T)$, $Ra=10^6$ (I3); (d) $\eta(T,Z)$, $Ra=10^6$ (I4); (e) constant viscosity, $Ra=10^5$ (I5); (f) $\eta(T,Z)$, $Ra=10^5$ (I6); (g) constant viscosity, $Ra=10^7$ (I7); and (h) $\eta(T,Z)$, $Ra=10^7$ (I8). Further details are given in Table 4.

from the region of downwelling. The contrast between this solution and case C1 provides a very clear demonstration of the ability of temperature dependent viscosity to produce long wavelength flows. The pattern has a similar wavelength to that obtained in the Boussinesq, basally heated cases B2 and B4.

With both temperature- and depth-dependent viscosity, downwelling is again restricted to one side of the box, where a downwelling sheet with time dependent plumelike instabilities is observed. This corresponds to an infinite series of sheetlike downwellings with horizontal spacing 8 (equivalent to ~23,000 km). Time dependent, linear extensions appear from these plumes into the hot upwelling region.

Constant-viscosity cases for two other Ra are presented (I5 and I7). At the lower Ra number, a much more stable pattern with fragmented downwelling sheets is formed. This appears to differ from low-Ra Boussinesq solutions, in which downwelling plumes are still obtained [*Schubert et al.*, 1993]. At the higher Ra, the basic characteristics are the same as for case C1, but the downwellings are narrower and more closely spaced.

Cases with temperature and depth dependent viscosity are also presented for two other Ra (case I6 at $Ra_T=10^5$ and case I8 at $Ra_T=10^7$), and can be compared to case I4. At the lower Ra, two steady state downwelling plumes have formed at opposing corners of the box, with the hot material filling in the gaps between these. At the higher Ra, however, a time dependent network of narrow plumelike downwellings is observed, connected by linear sheets. The spacing associated with these downwellings is smaller than with the case at $Ra=10^6$ (I4), although larger than the constant-viscosity case I7. This provides further evidence that the characteristic horizontal wavelength decreases with increasing Ra.

Vertical Versus Horizontal Viscosity Variations

When contemplating the large change in planform temperature dependent viscosity can cause, for example, from case B1 to case B2, the interesting question of what is the most important effect arises: is it vertical variations in viscosity (which arise because of the temperature dependence), horizontal variations in viscosity, or are fully three-dimensional viscosity variations necessary? This question is important because the most widely used methods for determining the viscosity profile of the mantle, namely, geoid modeling and the inversion of postglacial rebound data, are not sensitive to lateral variations in viscosity.

To address this question, two additional cases were performed, cases B9 and B10, which are the same as B2 except with averaging done on the viscosity field. In case B9, the full 3-D viscosity field is calculated at each time step as usual, but then averaged horizontally, giving only vertical viscosity variations. In case B10, the 3-D viscosity field is normalized by (divided by) the horizontal average at each z, so that viscosity variations are predominantly horizontal, with no vertical variation in the mean viscosity. The results are shown in Figure 5, which also shows a rerun of case B2 from a different initial condition. All three cases were started from a very short wavelength pattern, ensuring that the final planform was not caused by any bias in initial conditions. The convective pattern obtained in case B9 (with only vertical viscosity variations) is, to first order, the same as that obtained in case B2 (with fully 3-D viscosity variations). In contrast, the pattern obtained in case B10 (with mostly horizontal variations) is of much shorter wavelength, although also with upwelling sheets and downwelling plumes. Thus the dominant factor influencing the planform of temperature dependent viscosity 3-D convection is the mean depth dependence that arises from the temperature dependence.

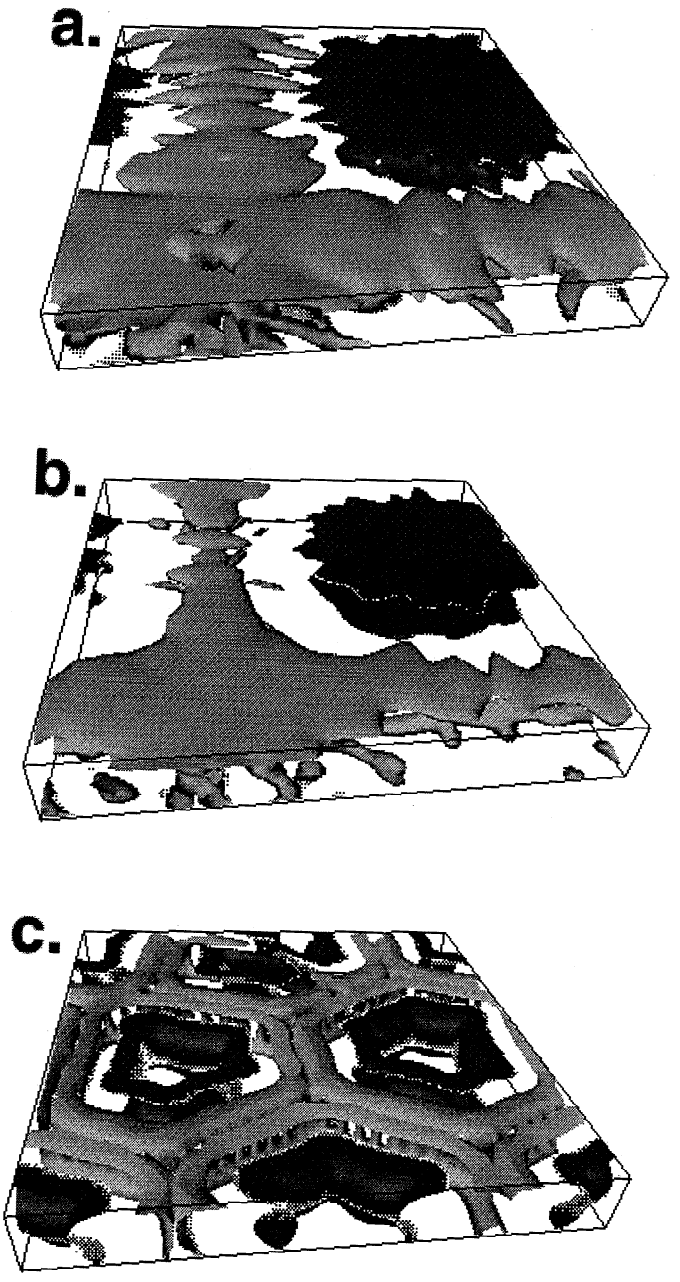

Figure 5. The effect of vertical and horizontal viscosity variations. (a) Full 3-D $\eta(T)$ (as case B2 but with RSC starting condition); (b) $\eta(T)$ but horizontally averaged to yield only vertical viscosity variations (case B9); (c) $\eta(T)$ normalized by the horizontal average to yield mostly horizontal viscosity variations (case B10).

Horizontally Averaged Properties

Figures 6 and 7 show vertical profiles of horizontally averaged temperature $<T>$, viscosity $<\eta>$, rms velocity (v_{rms}) and stress (i.e., $\sqrt{(\tau_{ij}\tau_{ij})}$), for the first two groups of cases. In each group the solid line represents the constant-viscosity case.

Boussinesq (Figure 6). The constant-viscosity case displays an approximately isothermal interior with $T \approx 0.5$, and upper and lower boundary layers have an approximately equal temperature drop and thickness of around 0.1, which is roughly $(Ra_c/Ra)^{1/3}$, where Ra_c is the critical Rayleigh number for the onset of convection. Since there is no adiabatic increase of temperature with depth in the Boussinesq approximation, this isotherm is equivalent to an adiabat. Regions of subadiabaticity are observed near the upper and lower boundary layers; these are due to the horizontal spreading of upwellings and downwellings at these depths. These regions are expected to become smaller as Ra increases, and the interior temperature profile would become closer to an isotherm, as with 2-D calculations [*Jarvis and Peltier,* 1989].

When depth dependence of viscosity is added (B5, dotted line in Figure 6), the interior temperature drops greatly to around 0.3, resulting in a lower thermal boundary layer with much greater temperature drop and vertical extent of around 0.25. The effect of depth-dependent viscosity in decreasing the interior temperature has previously been observed in two-dimensional simulations [*Torrance and Turcotte*, 1971; *Gurnis and Davies,* 1986; *Yuen and Zhang,* 1989; *Hansen et al.*, 1993]. The effect can be understood by noting that convection tends to be more vigorous where viscosity is lower. The lower viscosity towards the top of the layer results in more vigorous convection, and hence higher heat transport, near the top than near the base, thus cooling the interior until the temperature drops over upper and lower thermal boundary layers adjust to equalize the heat transport. Essentially, it is easier to transport heat through the surface than through the base.

When the viscosity is dependent only on temperature (cases B4 and B7), the upper boundary layer becomes stiff, heat transport is impeded, and the interior temperature rises to around 0.7 for the cases reported here. This increase of interior temperature due to temperature dependent viscosity has been noted in most of the previous laboratory and numerical studies discussed earlier. The interior of the cell is again approximately isothermal, with a marked cold region just above the lower thermal boundary layer, which is due to the horizontal spreading of the large cylindrical downwelling plumes. As Ra is increased from 10^5 to 10^6 (case B2 to B7), the boundary layers and this cold region become smaller in vertical extent, and the interior is more nearly isothermal.

The viscosity profiles for these cases display the same features. The interior mean viscosity for case B4 is greater than 1 even though the interior mean temperature is greater

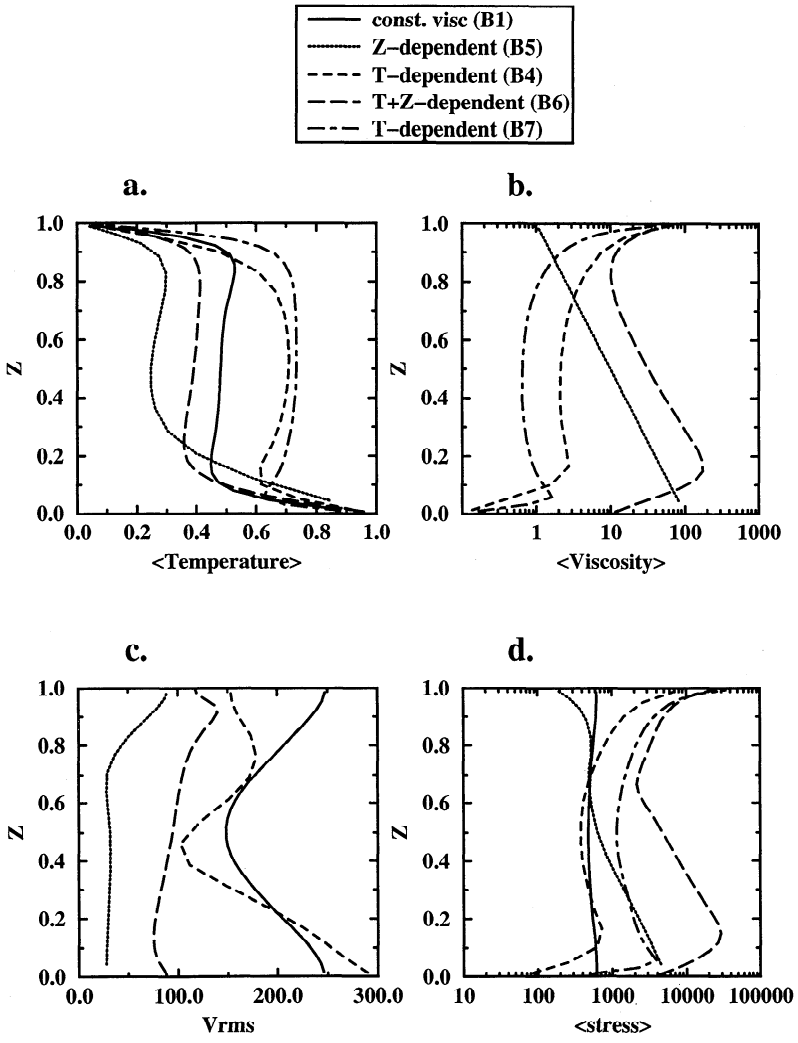

Figure 6. Profiles of (a) horizontally averaged temperature <T>, (b) dynamic viscosity <η>, (c) rms velocity V_{rms} and (d) stress, for Boussinesq, basally heated cases.

than 0.5, and $\eta(T=0.5)=1$. This is due to the fact that the exponential of the mean of some values is not the same as the mean of the exponential of the values, and the highly viscous cold downwelling plumes raise the horizontally averaged viscosity more above 1. If the geometric rather than arithmetic mean of the viscosity was used (equivalent to taking the mean in logarithmic space) as in *Christensen* [1985], this effect would be less pronounced, and the viscosity profile could be calculated directly from the mean temperature profile. In case B7, the narrower cold plumes associated with the higher *Ra* have a smaller effect on horizontally averaged viscosity, and thus $<\eta>$ is significantly lower than case B4, more so than would be predicted simply from the change in $<T>$.

Nataf [1991] observed that in laboratory experiments, the internal temperature adjusts so that the viscosity contrast over the lower boundary layer never exceeds a factor of about 8, regardless of the total viscosity contrast across the layer. In these 3-D simulations, a somewhat larger viscosity contrast of about 20 is obtained across the lower boundary layer. This difference could be due to the stress-free boundary conditions, as opposed to the rigid boundaries of laboratory experiments, or to differences in the viscosity law, which in these current simulations, gives much larger viscosity variations for cold regions than for hot regions. It would be interesting to progress to higher total viscosity contrasts, in order to establish whether the lower viscosity contrast would remain constant. Limitations in the numerical technique prevent this test for the moment, however.

Adding depth dependence to the temperature dependence of viscosity (case B6) reduces the interior temperature to about 0.4, resulting in a slightly subadiabatic internal temperature profile, and a systematic increase in viscosity with depth, except within the boundary layers. Thus it seems that the interior temperature of the mantle is quite sensitive to the exact details of the rheological law, and is a delicate balance between temperature dependence increasing the temperature and depth dependence decreasing the temperature.

The rms velocity profiles give an indication of convective vigor. When depth-dependent viscosity is included (cases B5 and B6), there is a systematic decrease in velocity with depth, as would be expected. Constancy of heat transport is obtained by the larger temperature drop over the lower boundary layer, resulting in larger horizontal temperature differences in the deep mantle, where circulation is sluggish. Temperature dependent viscosity (cases B4 and B6) causes a local decrease in velocity in the upper boundary layer and a local increase in velocity in the lower boundary layer. Flow is not greatly inhibited at the top, however, and the stiff upper boundary layer still participates in the flow, corresponding to the whole-mantle regime described by *Ogawa et al.* [1991].

Stress profiles appear closely related to the viscosity profiles, displaying the same features. The constant-viscosity case (B1) has approximately constant stress. Cases with temperature dependent viscosity display stress minima in the hot lower boundary layer and strong stress maxima at the surface. Indeed, the stress level at the surface is typically around 1.5-2 orders of magnitude larger than the stress in the interior of the cell. With depth-dependent viscosity included, there is an additional stress maximum in the lower mantle.

Compressible (Figure 7). The profiles for the constant-viscosity compressible case C1 display some marked differences from the Boussinesq case B1. As expected, the interior temperature now exhibits a gradient due to adiabatic compression. The interior temperature is also higher, with a much larger temperature drop over the upper boundary layer, although the boundary layers are of similar thickness.

Rough scaling relationships can be obtained by applying a local *Ra* criterion [*Howard*, 1966] to each boundary layer. The boundary layer *Ra* (i.e., defined using the thickness of the boundary layer as the length scale, the temperature drop over the boundary layer as the temperature scale, and local values of thermodynamic parameters) must be equal to the critical *Ra* for convective instability:

$$\frac{\rho_u \alpha_u \Delta T_u \delta_u^3}{\eta_u \kappa_u} \approx \frac{\rho_l \alpha_l \Delta T_l \delta_l^3}{\eta_l \kappa_l} \tag{12}$$

where δ is the boundary layer thickness, subscripts u and l denote upper and lower boundaries, respectively, and the other symbols were defined earlier. In addition, heat flow through top and bottom must be equal (noting that heat capacity is held constant):

$$\frac{\rho_u \kappa_u \Delta T_u}{\delta_u} \approx \frac{\rho_l \kappa_l \Delta T_l}{\delta_l} \tag{13}$$

leading to scalings for temperature

$$\frac{\Delta T_u}{\Delta T_l} \approx \frac{\rho_l}{\rho_u}\left(\frac{\kappa_l}{\kappa_u}\right)^{1/2}\left(\frac{\alpha_l \eta_u}{\alpha_u \eta_l}\right)^{1/4} \tag{14}$$

and boundary layer thickness

$$\frac{\delta_u}{\delta_l} \approx \left(\frac{\kappa_u}{\kappa_l}\right)^{1/2}\left(\frac{\alpha_l \eta_u}{\alpha_u \eta_l}\right)^{1/4} \tag{15}$$

For Boussinesq cases these simplify to

$$\frac{\Delta T_l}{\Delta T_u} = \frac{\delta_l}{\delta_u} \approx \left(\frac{\eta_l}{\eta_u}\right)^{1/4} \tag{16}$$

These scaling laws explain all the trends that have been observed in these and previous 2-D numerical simulations with depth-dependent parameters. Decreasing α or increasing η with depth reduces the interior temperature [*Gurnis and Davies*, 1986; *Yuen and Zhang*, 1989; *Hansen et al.*, 1993], and increasing k with depth increases the interior temperature [*Yuen and Zhang*, 1989; *Leitch et al.*, 1991]. For Boussinesq cases the scalings are quantitatively successful, giving a ratio of approximately 3 for the 100-fold viscosity increase used in case B5, approximately what is observed. For compressible cases, the formulae appear to give reasonable scaling with η but are less successful in predicting absolute values of ratios: for constant-viscosity case C1, we expect $\Delta T_u/\Delta T_l \approx 1.5$ and $\delta_u/\delta_l \approx 0.4$, both somewhat lower than observed (2.8 and 0.9, respectively); whereas for with a 100-fold viscosity increase (case C2), we expect $\Delta T_u/\Delta T_l \approx 0.5$ and $\delta_u/\delta_l \approx 0.125$, which are also too low by a similar factor ($\Delta T_u/\Delta T_l \approx 1.0$ and $\delta_u/\delta_l \approx 0.33$).

For the cases with viscosity variations (C2-C4), the same trends as for the Boussinesq cases can be observed, i.e., temperature dependence of viscosity increases interior temperature, and depth dependence decreases the interior

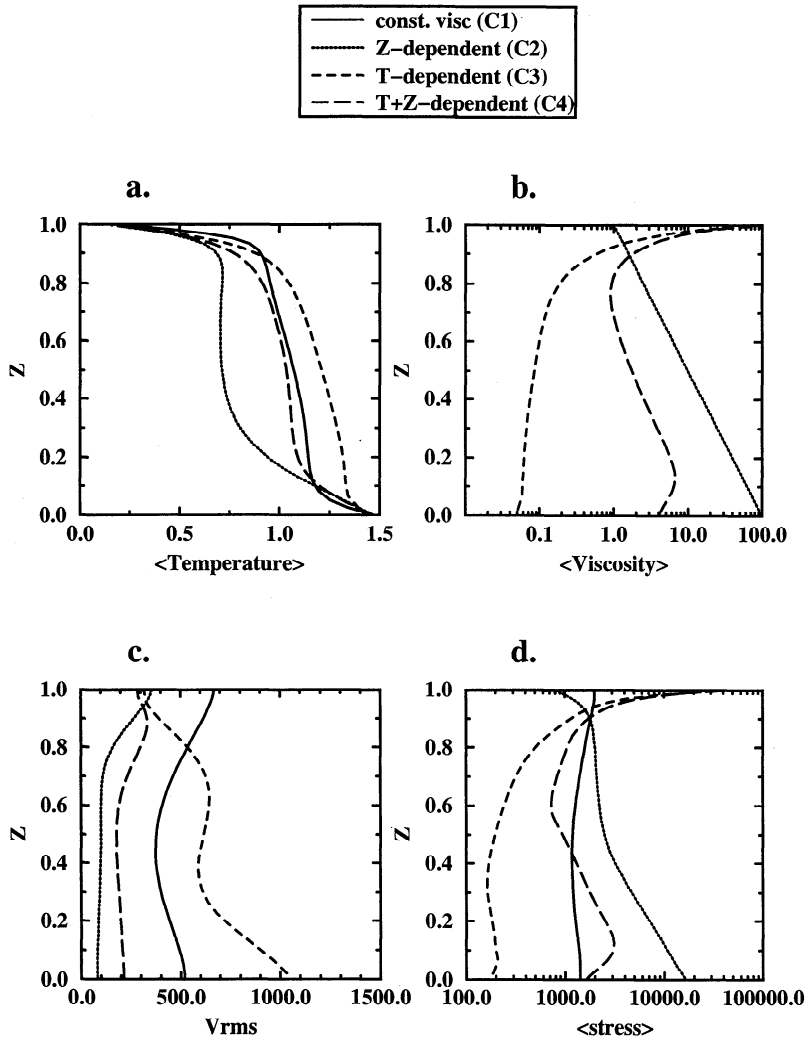

Figure 7. Profiles of (a) horizontally averaged temperature <T>, (b) dynamic viscosity <η>, (c) rms velocity V_{rms} and (d) stress, for compressible, basally heated cases.

temperature. For case C3, which has temperature dependent viscosity, the interior temperature is so high, that the temperature contrasts associated with upwellings are difficult to detect in images of the T field. In case C3, the adiabatic increase of temperature with depth results in a decrease of viscosity with depth, an effect which reduces the amount of viscosity increase with depth in case C4.

Velocities and stress also display the same trends as for the constant-viscosity cases. For the constant-viscosity case C1, circulation is somewhat more sluggish in the deep mantle than in the shallow mantle, presumably due to the decrease of local Ra caused by depth-dependent properties.

Internal heating The profiles obtained in the internally heated cases I1 to I4 are almost identical to those of cases C1 to C4 except for the absence of a lower thermal boundary layer and resulting slightly lower velocities and stresses in the deep mantle. Thus they are not presented in this paper.

Thermal Budget

Figure 8 shows the horizontally averaged heating (positive) or cooling (negative) rates due to the various terms in the energy equation (equation (3)), namely, advection, diffusion (second term on the right hand side), and the compressible terms adiabatic heating (AH, first term on the right hand side) and viscous dissipation (VD, last term on the right hand side), for various cases. These terms represent the divergence of the relevent heat fluxes. Similar information for spherical geometry is plotted in Figure 2 of *Glatzmaier* [1988]. The term "adiabatic heating" is somewhat misleading, since no entropy production is involved; the term arises simply from material moving up and down adiabats. Conservation of mass necessitates that the upward mass flux through a particular depth is equal to the downward mass flow through that depth. However, "hot" adiabats are steeper than "cold" adiabats; hence hot upwelling material will be adiabatically cooling as it rises more rapidly than cold downwelling material will be adiabatically warming as it descends. Thus the horizontally averaged adiabatic heating is negative. The term disappears when the thermal equation is written in terms of entropy rather than temperature [e.g., *Glatzmaier*, 1988]. Thermodynamic considerations [*Jarvis and Peltier,* 1989; *Hewitt et al.*, 1975; *Backus*, 1975] indicate that (1) the volume-integrated viscous

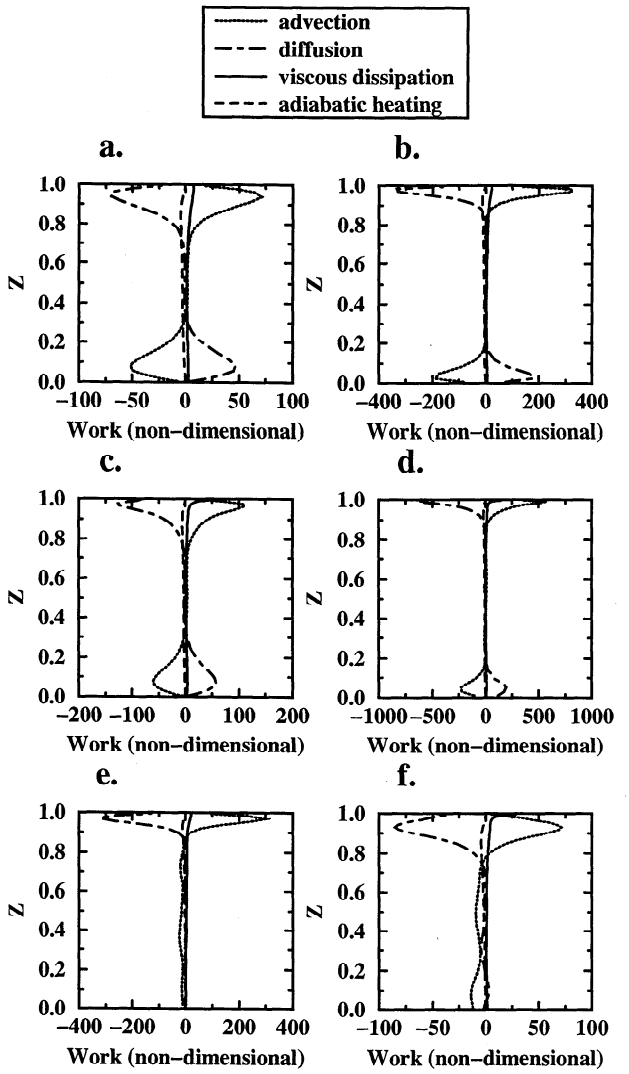

Figure 8. Heat balance for various cases. Plotted are depth profiles of the horizontally averaged values of the various terms in the temperature equation, representing the divergence of heat fluxes for advection, diffusion, viscous dissipation, and adiabatic heating. Constant-viscosity compressible cases (a) C8 ($Ra=10^5$) and (b) C1 ($Ra=10^6$), temperature- and depth-dependent viscosity compressible cases (c) C4 ($Ra=10^6$) and (d) C6 ($Ra=10^7$), and internally heated cases (e) I1 (constant viscosity, $Ra=10^6$) and (f) I4 (temperature- and depth-dependent viscosity, $Ra=10^6$).

dissipation is equal and opposite to the volume-integrated adiabatic cooling, (2) the ratio E of volume-integrated VD to surface heat flux is expected to be independent of Ra and (for basally heated convection) bounded by the dissipation number, as confirmed by *Jarvis and McKenzie* [1980], (3) this ratio can thus be much larger than 1 for dissipation numbers much greater than 1. Consideration 1 indicates that VD and AH have no net contribution to the heat flow through the mantle; they can merely be regarded as heat sources and sinks which redistribute heat in the interior. In this regard, *Jarvis and McKenzie* [1980], *Bercovici et al.* [1992], and *Balachandar et al.* [1993, 1995a,b] show that VD is concentrated in the boundary layers at the edges of upwellings and downwellings.

Constant viscosity. For the constant-viscosity cases, the dominant terms are observed to be advection and diffusion, which have large peaks in the boundary layers. The additional terms associated with compressibility (VD and AH) play only a minor role in the heat budget for these cases. All of the contributions to heat budget increase with Ra. Advection and diffusion also become more localized towards the boundaries, due to the narrower boundary layers. *Balachandar et al.* [1993] state that VD and AH become more important at higher Ra, and the results presented here confirm that these terms increase with Ra. However, the peak values for advection and diffusion increase equally or more rapidly with Ra than the peak values for VD and AH. Thus relative to the overall heat budget, AH and VD do not become more important as Ra increases.

A simple scaling analysis, based on the idealized scaling of Nusselt number ($Ra^{1/3}$), velocity ($Ra^{2/3}$), and boundary layer thickness ($Ra^{-1/3}$) [*Turcotte and Schubert*, 1982], supports these observations. Advection and diffusion terms scale as the Nusselt number, i.e., $Ra^{1/3}$. Adiabatic heating scales as the velocity ($Ra^{2/3}$) times the width of convective features ($Ra^{-1/3}$), resulting in a $Ra^{1/3}$ scaling. Since the velocity field fills the domain even for highly concentrated thermal features [*Jarvis and Peltier*, 1989] the appropriate length scale for strain rate is D, and thus strain rate and nondimensional stress (because $\eta \equiv 1$) scale in proportion to velocity, i.e., $Ra^{2/3}$. Nondimensional viscous dissipation is the product of these divided by Ra (see equation (3)), resulting in an overall $Ra^{1/3}$ scaling for this term. Thus all terms are expected to increase by similar amounts with increasing Ra (i.e., as $Ra^{1/3}$), as observed in the presented simulations, and predicted by more rigorous theory [*Hewitt et al.*, 1975]. If flow were highly localized, which is not the case in the constant-viscosity results, but may become true when temperature dependent viscosity in included [*Balachandar et al.*, 1995a], the appropriate length scale in the strain rate would be smaller. Since the local magnitude of viscous dissipation changes as (1/length scale)^2, viscous dissipation may then become important in local regions [*Balachandar et al.*, 1995a,b].

T-dependent viscosity. The addition of temperature dependent viscosity results in a large increase in horizontally averaged viscous dissipation towards the upper surface. The magnitude of VD is now comparable to that of the advection and diffusion terms. The increase of VD with temperature dependent viscosity has been noted in the 3-D calculations of *Balachandar et al.* [1995a,b]. The peak in viscous dissipation arises from the stress peak in the upper boundary layer noted in the discussion of radial profiles. Note that the volume-integrated VD is still bound by thermodynamic considerations to be equal and opposite to volume-averaged adiabatic cooling; temperature dependent viscosity has merely concentrated it in the upper boundary layer.

For the internally heated cases (Figures 8e and 8f), peak values of the horizontally averaged advection and diffusion are very much larger than the internal heating rate (16 and 10, respectively). With temperature dependent viscosity, peak values of VD can also be larger than the internal heating rate (Figure 8f), as pointed out by *Balachandar et al.* [1995b]. However, in a volume-averaged sense, viscous dissipation is still a minor component in the heat budget.

Discussion

Hot Sheets and Coldspots?

The upwelling sheets and downwelling plumes found in the basally heated cases with purely temperature dependent viscosity (B2, B3, B4, and C3) are compatible with the result obtained by *Weinstein and Christensen* [1991] in a 4x4x1 box with rigid lower and stress-free (isothermal) upper boundaries, and a viscosity contrast of 50. The pattern can be understood in the following terms. Depth-dependent properties cause the local *Ra* to decrease with depth, resulting in large cells with downwelling sheets and upwelling plumes (case C1 and *Balachandar and Yuen* [1992]). In the present, temperature dependent viscosity cases (B2, B3, B4, and C3), the opposite occurs, i.e., the local *Ra* increases by 3 orders of magnitude with depth. Thus, the inverse flow pattern is obtained: upwelling sheets and downwelling plumes, with the viscous upper boundary layer imposing a long wavelength to the flow.

Are such upwelling sheets likely in the Earth? For example, it may be tempting to interpret these upwelling sheets as possible active deep upwelling below mid-ocean ridges. However, this would violate constraints from geoid, topography, and heat flow [*Davies*, 1988]. Other results presented here show that adding greater realism in the form of depth-dependent viscosity and/or internal heating and/or compressibility, pushes the system towards a preference for upwelling plumes. Spherical geometry is likely to work in the same direction. Thus it seems likely that for realistic material properties, heating mode, and geometry, upwelling plumes, rather than narrow upwelling sheets, will be the preferred mode of upwelling.

On Earth, the major downwellings seem to occur exclusively as linear slabs: cylindrical "coldspots" are not observed. This may be a natural consequence of plate tectonics and the associated complete subduction of rigid lithosphere by means faults in the crust and lithosphere. It is difficult to imagine a fault system that would allow a rigid plate to converge radially from all directions into a common coldspot, without the system being extremely dissipative. On Venus, however, plate tectonics is not currently operative, and quasi-cylindrical downwellings may well occur below a rigid or slowly deforming lid. Indeed, plateau-shaped highlands found in regions such as Aphrodite Terra or Ishtar Terra have been associated with cold cylindrical downwellings by some researchers [*Kiefer and Hager*, 1991; *Bindschadler et al.*, 1992].

Horizontal Wavelengths

A considerable variation in characteristic horizontal wavelengths is observed, depending on the material properties and heating mode. Temperature dependent viscosity with no depth dependence favors very broad cells (wavelength ≥ 8). However, adding depth dependence results in very small cells (wavelength of order 1). Compressibility acts in the opposite direction, increasing the cell size.

It is important to consider how the limited domain size in these experiments (usually an aspect ratio 4 box with reflecting sides) constrains the observed horizontal wavelengths and planform. The constraints are threefold: (1) the maximum cell wavelength is 8, (2) the actual wavelength is 8 or an integer subdivision of 8, for example, 4, 8/3, 2, 8/5, etc., and (3) there is a greatly enhanced tendency for cells to be square, as opposed to, for example, hexagonal. Case B3, in an aspect ratio 8 box with reflecting sides, suggests that constraint 1 is not a problem, since the flow could have adopted a wavelength of 16 but instead chose one that is close to 8. Limitations 2 and 3 are likely to be strong constraints only when the flow wavelength approaches the size of the box, which it does in many of these experiments. However, the general type of flow pattern (e.g., upwelling sheets, downwelling plumes) and the rough order-of-magnitude cell size, are unlikely to be affected by these limitations, as demonstrated by case C9 compared to case C1.

These effects may be understood in terms of a competition between boundary layers, in the regime where both boundary layers are mobile (as is the case in all of the basally heated results in this paper). When one boundary layer is much more sluggish than the other, which could be the upper boundary layer in a Boussinesq case with temperature dependent viscosity, or the lower boundary layer in a case with constant viscosity but depth-dependent compressible parameters, long wavelength cells result. However, when both boundary layers are of similar stiffness, as in the Boussinesq case with depth- and temperature dependent viscosity (B6), short-wavelength cells result. In internally heated cases, the important competition is between the interior of the convective cell, which wants to adopt an aspect ratio of order unity, and the sluggish upper boundary layer, which is advected along with the general flow but, due to its high viscosity, takes a long time to become unstable, resulting in long cells. When the upper boundary layer becomes completely immobile due to very high viscosity [*Giannandrea and Christensen*, 1993] or a rigid boundary condition [*Tackley*, 1993], this argument does not apply, and cells with aspect ratio of order unity result.

Rayleigh number also appears to play a role in determining horizontal length scales, particularly when one or more depth-dependent properties are present. A decrease in cell size with an order-of-magnitude increase in *Ra* was noted when viscosity was dependent on temperature and pressure for Boussinesq cases (B6 and B8), for compressible, basally heated cases (B4 and B6), and for compressible, internally heated cases (I4 and I8). A decrease was also noted for constant-viscosity, compressible, internally heated cases (I5, I1, and I7). More tests are needed to establish whether this trend holds true for all combinations of parameters. *Hansen et al.* [1993] found using steady state 2-D calculations that temperature dependent viscosity has less influence on the convection as *Ra* is increased with a fixed viscosity contrast. The results presented here indicate that temperature dependent viscosity tends to result in large cells, compared to constant-viscosity cases. If the viscosity variations had less effect at higher *Ra*, the cell size might decrease towards the size observed in constant-viscosity cases. This mechanism may be particularly appropriate for explaining the difference between case I1 and case I7. Since the viscosity contrast in the mantles of Earth or Venus is likely to be much higher than that modeled here, however, this trend may not be relevant to planetary mantles.

Upwelling Plume Character

These results indicate that including a viscosity which is dependent on temperature alone does not lead to upwelling

plumes, but rather upwelling sheets (e.g., cases B2 and C3), with downwellings being plumelike. The addition of depth dependence to the viscosity law (or constant viscosity and depth-dependent material properties, e.g., case C1), is necessary for plumes to be the dominant mode of upwelling (e.g., cases B6 and C4). The following discussion refers to such cases.

Temperature dependent viscosity results in a low-viscosity layer immediatcly abovc thc CMB, strongly affecting the formation and dynamics of upwelling plumes [*Sleep*, 1987; *Olson et al.*, 1987, 1993]. Popular models for plumes in the Earth (for summaries, see *Loper* [1991] and *Duncan and Richards* [1991]) assume that plume conduits are uniformly narrow throughout thc depth of thc mantlc. In global seismic tomographic models [*Su et al.*, 1994; *Fukao*, 1992], very broad hot regions, resembling vast upwelling plumes, are observed in the lower mantle, although since narrow plumes cannot be detected in such models, it is not clear whether these regions should be interpreted as single plumes, or simply as hot regions through which concentrated narrow plumes are rising.

In the compressible cases presented here, upwelling plumes are very broad, even when temperature dependent viscosity is included, more closely resembling those of seismic tomography than the idealized models. However, temperature dependent viscosity is observed to narrow the plumes (compare cases C2 and C4), and the viscosity contrast associated with plumes in these results is much smaller than that likely to be appropriate for the Earth because (1) numerical considerations limit the total viscosity contrast that can be modeled, (2) the Arrhenius law used results in larger viscosity variations in cold features than in hot features, and (3) when no mechanism for producing mobile surface plates and subduction is included, the viscosity contrast over the lower thermal boundary layer remains low even when the total viscosity contrast across the layer is increased [*Nataf*, 1991]. Thus the hot plumes in these models would be expected to become much narrower if a more realistic rheology and plates were included.

However, even with a more realistic viscosity contrast, plumes would still be broader at their base, narrowing as they ascend. This is due to the depth dependence of material properties, particularly thermal expansivity and thermal conductivity, which result in a decrease of the local Rayleigh number by at least an order of magnitude over the depth of the mantle. The likely increase in horizontally averaged viscosity with depth by 1-3 orders of magnitude would further reduce the local *Ra* by the same factor, resulting in an overall 2-4 order of magnitude decrease in local *Ra* over the depth of the mantle. Despite the large, first-order effect on plumc dynamics that this decrease would have, our current understanding of plumes is based on laboratory experiments [e.g., *Griffiths and Campbell*, 1990] and numerical and analytical models of plume formation, growth and propagation though mantle [e.g., *Olson et al.*, 1993; *Sleep*, 1990], which assume constant-properties (except for temperaturc dependent viscosity). The true picture of mantle plumes may be significantly different from the simple models on which our current understanding is based.

Internal Heating

The Earth's mantle is thought to be mainly internally heated [*Schubert*, 1979; *Davies and Richards*, 1992] and indeed, first-order evidence for this can be obtained by looking at surface observables: oceanic plates have a temperature anomaly of ~1300 K [*Turcotte and Schubert*, 1982] and account for ~75% of the heat loss from the interior [*Sclater et al.*, 1980], whereas hotspots, which are generally thought to be associated with hot upwelling plumes, have a much smaller thermal anomaly of only ~300 K in the upper mantle (although this temperature contrast may not be a good guide to the temperature drop over the lower thermal boundary layer) and account for only ~5-20% of the total heat loss [*Davies*, 1988; *Sleep*, 1990; *Davies and Richards*, 1992]. However, it has long been a problem that mantle convection simulations with large amounts of internal heating display a short-wavelength pattern of closely spaced, time dependent downwelling plumes, therefore resembling the Earth less than the downwelling sheets obtained in basally heated simulations (cases I1, I7 [*Houseman*, 1988; *Travis et al.*, 1990a; *Schubert*, 1992; *Parmentier et al.*, 1994]). These results show that variable viscosity provides a way of reconciling the observation of long wavelength flow with internal heating. Long wavelength flows are obtained even with internal heating, and there is a greater propensity for the downwellings to be linear, similar to slabs. In one result (case I2) with depth-dependent viscosity, when residual temperature (i.e., relative to geotherm) was plotted, a very broad hot upwelling "plume", somewhat reminiscent of those observed under the Pacific and Africa in global seismic tomographic models [e.g., *Su et al.*, 1994; *Fukao*, 1992], was visible, even though there was no heat being conducted through the core-mantle boundary. This indicates that the large plumes apparently observed in tomographic models are not necessarily indicative of high basal heat flux or vigorous upwelling; they may merely correspond to areas that have not been cooled by downwelling slabs [*Ricard et al.*, 1993].

Stagnant Lid and Non-Newtonian Rheology

In these simulations, the upper boundary layer participates in the flow. If the viscosity contrast were increased sufficiently, a "stagnant lid" would develop [*Ogawa et al.*, 1991], and the convective pattern might resemble the rigid boundary case, with small cells [*Giannandrea and Christensen*, 1993]. The current calculations lie in a regime which is transitional between the constant viscosity and asymptotic rigid lid regimes [*Solomatov*, 1995; *Moresi and Solomatov*, 1995]. However, the mobility of plates on the Earth suggest that the rigid lid regime is not relevant to Earth dynamics, even though the viscosity contrast over the lithosphere should be extremely large and is expected to place the Earth in this regime. On Venus, the high surface temperature and widespread tectonic deformation [*Solomon et al.*, 1992] also raise doubts about the relevance of this regime.

A rheological complexity which is expected to be important in some regions of the Earth's mantle and lithosphere is nonlinear (non-Newtonian) creep [*Kirby and Kronenberg*, 1987; *Karato and Wu*, 1993]. This has the effects of (1) generally reducing the viscosity contrast from that obtained using purely temperature dependent rheology [*Christensen*, 1984] (although the viscosity contrast in the presented results is already greatly reduced from a "realistic" value), (2) increasing the time dependence and irregular nature of the flow [*Christensen and Yuen*, 1989; *Malevsky and Yuen*, 1992], and (3) possibly inducing somewhat plate-like behavior in the stiff upper boundary layer [*Christensen and Harder*, 1991;

Weinstein and Olson, 1992; *Bercovici*, 1993]. Although the code is capable of modeling non-Newtonian creep [*Tackley*, 1993], it has been omitted in the presented results so that a thorough understanding of convection with linear creep can be obtained first.

Conclusions

These results show that a considerable range of convective styles and characteristic horizontal wavelengths is possible, depending on the exact details of rheology, compressibility, heating mode, and Rayleigh number. All of these have a significant effect on the flow, indicating the importance of including them into numerical models, and matching the Earth's parameter space as closely as possible.

Results obtained under the Boussinesq approximation show clearly the importance of modeling wide domains. With rheology being dependent solely on temperature and stress-free boundaries, very wide cells are formed (periodicity 8) with upwelling sheets and downwelling plumes, in contrast to the small-wavelength spoke pattern obtained with rigid boundaries [*White*, 1988; *Tackley*, 1993]. *Christensen and Harder* [1991] previously concluded that upwelling sheets are unlikely to occur in temperature dependent viscosity convection. However, these results indicate that at sufficiently large aspect ratio and with stress-free boundaries, they are the preferred solution. Adding depth dependence completely reverses these characteristics, resulting in small cells with upwelling plumes and downwelling sheets. Increasing the Rayleigh number by an order of magnitude does not appear to fundamentally change the convective pattern, resulting in narrower features and greater time dependence, and in some cases, smaller cell sizes. To first order, changes in planform arising from temperature dependent viscosity are due mainly to the mean depth dependence introduced by temperature dependence.

Compressibility, with the associated depth-dependent material properties, results in fairly large cells for basally heated models, and a preference for large upwelling plumes and narrow downwelling sheets. However, when the viscosity is dependent solely on temperature, downwelling plumes and linear upwellings are observed, in accordance with the equivalent Boussinesq solutions.

Perhaps the greatest modulation effect of viscosity variations occurs in internally heated, compressible cases. It is thought that the Earth and Venus are dominantly internally heated; however, constant-viscosity internally heated convection models display short-wavelength, highly time dependent cold plumes, which look less like the Earth than the downwelling sheets and upwelling plumes obtained in basally heated models. However, when the viscosity is dependent on temperature and/or depth, the planform is substantially changed to a long-wavelength pattern consisting of downwelling sheets at the surface with plume-like instabilities as they descend. Thus internally heated models are compatible with the Earth observations, provided an appropriate rheological law is used.

The temperature in the interior of convection cells, and the associated temperature drops over upper and lower boundary conditions, are strongly affected by the exact values of rheological and thermodynamic parameters. The interior temperature is strongly increased by temperature dependent viscosity and depth-dependent thermal conductivity, but strongly decreased by depth-dependent viscosity. This further illustrates the importance of trying to match the Earth's parameters as closely as possible. However, the temperature dependence of viscosity in the Earth is much stronger than in these simulations, which acts to buffer the interior temperature through a self-regulation mechanism first described by *Tozer* [1972], and thus the effect of various parameters on the internal mantle temperature may be lower than that predicted by these simulations. The interior temperature profile (away from boundary layers) is always close to adiabatic, and usually somewhat subadiabatic.

The convective vigor, as measured by rms velocity, is diminished in regions of high viscosity. However, in these calculations, the stiff upper boundary layer still participates in the flow; a larger viscosity contrast would be necessary to cause a rigid lid. The stress distribution resembles the viscosity distribution, with very high stress levels in the upper boundary layer.

Examination of the energy balance reveals that viscous dissipation and adiabatic heating are only minor contributors to the heat budget for constant-viscosity compressible mantle convection, with advection and diffusion playing the dominant role. Although the magnitude of viscous dissipation and adiabatic heating terms increases with Rayleigh number, advection and diffusion terms increase by a similar or larger factor, and thus viscous dissipation and adiabatic heating are still relatively unimportant. However, when temperature dependent viscosity is included, viscous dissipation becomes important in the stiff upper boundary layer due to the high stresses.

In these results, realistic plates and subduction are not obtained. Temperature dependent viscosity by itself does not result in plate-like behavior. The downwellings are two-sided, and a concentration of stress occurs where they leave the upper boundary layer. In order for plates to occur, an additional mechanism is needed to create weak zones in the stiff lid, such as nonlinear powerlaw rheology [*Cserepes*, 1982; *Christensen*, 1984; *Weinstein and Olson,* 1992], or a "stick-slip" rheology [*Bercovici*, 1993, 1995]. A priority in future work must be to examine the influences of these rheologies in self-consistent three-dimensional models. Other priorities include the effects of phase transitions, spherical geometry, compositional variations, and continents. Other possible rheological complexities not considered here include power law, non-Newtonian creep in the upper and possibly lower mantle [*Kirby and Kronenberg,* 1987; *Karato and Wu*, 1993], a viscosity jump at or around the 670-km discontinuity [*Hager and Richards,* 1989; *King and Masters*, 1992; *Forte et al.*, 1993; *Mitrovica and Peltier,* 1993], a hard garnet layer leading to higher viscosities in the transition zone [*Meade and Jeanloz*, 1990], and transformational superplasticity [*Karato and Li,* 1992].

Acknowledgments. Calculations were performed on the Intel Paragon at the San Diego Supercomputer Center, the Intel Touchstone Delta at the California Institute of Technology, and the Intel Paragon at the University of Hiroshima. The author thanks David Stevenson and Slava Solomatov for useful comments, and Mark Richards, Ulrich Christensen, and Louise Kellogg for constructive reviews. Supported by NSF grant EAR9017893

References

Anderson, D.L., A seismic equation of state, II., Shear properties and thermodynamics of the lower mantle, *Phys. Earth Planet. Inter., 45*, 307-323, 1987.

Anderson, O.L., H. Oda, and D. Isaak, A model for the computation of thermal expansivity at high compression and high temperatures: MgO as an example, *Geophys. Res. Lett., 19,* 1987-1990, 1992.

Backus, G.E., Gross thermodynamics of heat engines in the deep interior of the Earth, *Proc. Natl. Acad. Sci. U.S.A., 72,* 1555-1558, 1975.

Balachandar, S., and D.A. Yuen, Time-dependent three-dimensional compressible convection with depth-dependent properties, *Geophys. Res. Lett., 19,* 2247-2250, 1992.

Balachandar, S., D.A. Yuen, and D. Reuteler, Viscous and adiabatic heating effects in 3-dimensional compressible convection at infinite Prandtl number, *Phys. Fluids A, 5,* 2938-2945, 1993.

Balachandar, S., D.A. Yuen, and D.M. Reuteler, Localization of toroidal motion and shear heating in 3-D high Rayleigh number convection with temperature dependent viscosity, *Geophys. Res. Lett., 22,* 477-480, 1995a.

Balachandar, S., D.A. Yuen, D.M. Reuteler, and G.S. Lauer, Viscous dissipation in 3-dimensional convection with temperature dependent viscosity, *Science, 267*, 1150-1153, 1995b.

Baumgardner, J.R., Three-dimensional treatment of convective flow in the Earth's mantle, *J. Stat. Phys., 39,* 501-511, 1985.

Baumgardner, J.R., Application of supercomputers to 3-D mantle convection, in *The Physics of the Planets,* edited by S.K. Runcorn, pp. 199-231, John Wiley, New York, 1988.

Bercovici, D., A simple model of plate generation from mantle flow, *Geophys. J. Int., 114,* 635-650, 1993.

Bercovici, D., A source-sink model of the generation of plate tectonics from non-Newtonian mantle flow, *J. Geophys. Res., 100,* 2013-2030, 1995.

Bercovici, D., G. Schubert, and G.A. Glatzmaier, Influence of heating mode on three-dimensional mantle convection, *Geophys. Res. Lett., 16,* 617-620, 1989a.

Bercovici, D., G. Schubert, and G.A. Glatzmaier, Three-dimensional spherical models of convection in the Earth's mantle, *Science, 244,* 893-1016, 1989b.

Bercovici, D., G. Schubert, G.A. Glatzmaier, and A. Zebib, Three-dimensional convection in a spherical shell, *J. Fluid Mech., 206*, 75-204, 1989c.

Bercovici, D., G. Schubert, and G.A. Glatzmaier, Three-dimensional convection of an infinite-Prandtl-number compressible fluid in a basally heated spherical shell, *J. Fluid Mech., 239*, 683-719, 1992.

Bindschadler, D.L., G. Schubert, and W.M. Kaula, Coldspots and hotspots: Global tectonics and mantle dynamics of Venus, *J Geophys. Res., 97*, 13,495-13,532, 1992.

Blankenbach, B., et al., A benchmark comparison for mantle convection codes, *Geophys. J. Int., 98,* 23-38, 1989.

Booker, J.R., Thermal convection with strongly temperature dependent viscosity, *J. Fluid Mech., 76*, 741-754, 1976.

Boussinesq, J., *Théorie Analytique de la Chaleur Mise en Harmonie Avec la Thermodynamique et avec la Théorie Mécanique de la Lumière, vol. II,* pp. 157-176, Gauthier-Villars, Paris, 1903.

Brandt, A., Guide to multigrid development, in *Multigrid Methods: Proceedings Koln-Porz, 1981, Lecture Notes in Mathematics,* edited by W. Hackbusch and U. Trottenberg, pp 220-312, Springer-Verlag, New York, 1982.

Breuer, D., and T. Spohn, Cooling of the Earth, Urey ratios, and the problem of potassium in the core, *Geophys. Res. Lett., 20*, 1655-1658, 1993.

Busse, F.H., On the stability of two-dimensional convection in a layer heated from below, *J. Math. Phys., 46,* 140-150, 1967.

Busse, F.H., and H. Frick, Square-pattern convection in fluids with strongly temperature dependent viscosity, *J. Fluid Mech., 150*, 451-465, 1985.

Busse, F. H., et al., 3D convection at infinite Prandtl number in Cartesian geometry—A benchmark comparison, *Geophys. Astrophys. Fluid Dyn., 75,* 39-59, 1994.

Carrigan, C.R., Convection in an internally heated, high Prandtl number fluid: A laboratory study, *Geophys. Astrophys. Fluid Dyn., 32,* 1-21, 1985.

Chopelas, A., and R. Boehler, Thermal expansivity in the lower mantle, *Geophys. Res. Lett., 19*, 1983-1986, 1992.

Christensen, U.R., Convection with pressure- and temperature dependent non-Newtonian rheology, *Geophys. J. R. Astron. Soc., 77*, 343-384, 1984.

Christensen, U.R., Heat transport by variable viscosity convection, II; Pressure influence, non-Newtonian rheology and decaying heat sources, *Phys. Earth Planet. Inter., 37*, 183-205, 1985.

Christensen, U., and H. Harder, 3-D convection with variable viscosity, *Geophys. J. Int., 104,* 213-226, 1991.

Christensen, U. R., and D. A. Yuen, Time-dependent convection with non-Newtonian viscosity, *J. Geophys. Res., 94,* 814-820, 1989.

Cserepes, L., Numerical studies of non-Newtonian mantle convection, *Phys. Earth Planet. Inter., 30*, 49-61, 1982.

Cserepes, L., and U. Christensen, Three-dimensional convection under drifting plates, *Geophys. Res. Lett., 17*, 1497-1500, 1990.

Cserepes, L., M. Rabinowicz, and C. Rosemberg-Borot, Three-dimensional infinite Prandtl number convection in one and two layers with implications for the Earth's gravity field, *J. Geophys. Res., 93*, 12,009-12,025, 1988.

Davies, G.F., Ocean bathymetry and mantle convection, 1, Large-scale flow and hotspots, *J. Geophys. Res., 93,* 10467-10480, 1988.

Davies, G.F., and M.A. Richards, Mantle convection, *J. Geology, 100,* 151-206, 1992.

Duffy, T.S., and T.J. Ahrens, Thermal expansion of mantle and core materials at very high pressures, *Geophys. Res. Lett., 20*, 1103-1106, 1993.

Duncan, R.A., and M.A. Richards, Hotspots, mantle plumes, flood basalts, and true polar wander, *Rev. Geophys., 29,* 31-50, 1991.

Durham, W.B., C. Froidevaux, and O. Jaoul, Transient and steady state creep of pure forsterite at low stress, *Phys. Earth Planet. Inter., 19*, 263-274, 1979.

Dziewonski, A.M., and D.L. Anderson, Preliminary reference Earth model, *Phys. Earth Planet. Inter., 25,* 297-356, 1981.

Forte, A.M., A.M. Dziewonski, and R.L. Woodward, Aspherical structure of the mantle, tectonic plate motions, nonhydrostatic geoid, and topography of the core-mantle boundary, in *Dynamics of the Earth's Deep Interior and Earth Rotation, Geophys. Monogr., vol 72,* edited by J.L. LeMouel, D.E. Smylie, and T. Herring, pp. 135-166, AGU, Washington, D.C., 1993.

Frick, H., F.H. Busse, and R.M. Clever, Steady three-dimensional convection at high Prandtl numbers, *J. Fluid Mech., 127*, 141-153, 1983.

Fukao, Y., Seismic tomogram of the Earth's mantle: Geodynamic implications, *Science, 258*, 625-630, 1992.

Gable, C.W., R.J. O'Connell, and B.J. Travis, Convection in three dimensions with surface plates: Generation of toroidal flow, *J Geophys. Res., 96,* 8391-8405, 1991.

Giannandrea, E., and U. Christensen, Variable viscosity convection experiments with a stress-free upper boundary and implications for the heat transport in the Earth's mantle, *Phys. Earth Planet. Inter., 78*, 139-152, 1993.

Glatzmaier, G.A., Numerical simulations of mantle convection: Time-dependent, three-dimensional, compressible, spherical shell, *Geophys. Astrophys. Fluid Dyn., 43*, 223-264, 1988.

Glatzmaier, G.A., and G. Schubert, Three-dimensional spherical models of layered and whole mantle convection, *J. Geophys. Res., 98*, 21,969-21,976, 1993.

Glatzmaier, G.A., G. Schubert, and D. Bercovici, Chaotic, subduction-like downflows in a spherical model of convection in the Earth's mantle, *Nature, 347*, 274-277, 1990.

Griffiths, R.W., and I.H. Campbell, Stirring and structure in mantle plumes, *Earth Planet. Sci. Lett., 99*, 66-78, 1990.

Gurnis, M., and G.F. Davies, Numerical study of high Rayleigh number convection in a medium with depth-dependent viscosity, *Geophys. J. R. Astron. Soc., 85,* 523-541, 1986.

Hager, B.H., and M.A. Richards, Long-wavelength variations in Earth's geoid: Physical models and dynamical implications, *Philos. Trans. R. Soc. London., 328*, 309-327, 1989.

Hansen, U., D.A. Yuen, S.E. Kroening, and T.B. Larsen, Dynamical consequences of depth-dependent thermal expansivity and viscosity on mantle circulations and thermal structure, *Phys. Earth Planet. Inter., 77,* 205-223, 1993.

Hewitt, J.M., D.P. McKenzie, and N.O. Weiss, Dissipative heating in convective flows, *J. Fluid Mech., 68,* 721-738, 1975.

Honda, S., D.A. Yuen, S. Balachandar, and D. Reuteler, Three-dimensional instabilities of mantle convection with multiple phase transitions, *Science, 259,* 1308-1311, 1993.

Houseman, G., The dependence of convection planform on mode of heating, *Nature, 332,* 346-349, 1988.

Howard, L.N., Convection at high Rayleigh number, in *Proceedings of the Eleventh International Congress of Applied Mechanics,* edited by H. Gortler, pp. 1109-1115, Springer-Verlag, New York, 1966.

Jarvis, G.T., and D.P. McKenzie, Convection in a compressible fluid with infinite Prandtl number, *J. Fluid Mech., 96,* 515-583, 1980.

Jarvis, G.T., and W.R. Peltier, Convection models and geophysical observations, in *Mantle Convection: Plate Tectonics and Global Dynamics* edited by W.R. Peltier, pp. 479-594, Gordon and Breach, New York, 1989.

Karato, S., and P. Li, Diffusion creep in perovskite—Implications for the rheology of the lower mantle, *Science, 255,* 1238-1240, 1992.

Karato, S., and P. Wu, Rheology of the upper mantle: A synthesis, *Science, 260,* 771-778, 1993.

Kiefer, W.S., and B.H. Hager, Mantle downwelling and crustal convergence—A model for Ishtar Terra, Venus, *J. Geophys. Res., 96*, 967-980, 1991.

King, S. D., and G.T. Masters, An inversion for radial viscosity structure using seismic tomography, *Geophys. Res. Lett., 19*, 1551-1554, 1992.

Kirby, S.H., and A.K. Kronenberg, Rheology of the lithosphere: Selected topics, in *US National Report to International Union of Geodesy and Geophysics 1983-1986, Contributions in Tectonophysics,* pp. 1219-1244, AGU, Washington, D.C., 1987.

Leitch, A.M., D.A. Yuen, and G. Sewell, Mantle convection with internal heating and pressure-dependent thermal expansivity, *Earth Planet. Sci. Lett., 102,* 213-232, 1991.

Loper, D.E., Mantle plumes, *Tectonophysics, 187,* 373-384, 1991.

Machetel, P., M. Rabinowicz, and P. Bernardet, Three-dimensional convection in spherical shells, *Geophys. Astrophys. Fluid Dyn., 37*, 57-84, 1986.

Malevsky, A. V., and D. A. Yuen, Strongly chaotic non-Newtonian mantle convection, *Geophys. Astrophys. Fluid Dyn., 65*, 149-171, 1992.

Malevsky, A.V., and D.A. Yuen, Plume structures in the hard-turbulent regime of three-dimensional infinite Prandtl number convection, *Geophys. Res. Lett., 20,* 383-386, 1993.

Meade, C., and R. Jeanloz, The strength of mantle silicates at high pressures and room temperature: Implications for the viscosity of the mantle, *Nature, 348*, 533-535, 1990.

Mitrovica, J.X., and W.R. Peltier, The inference of mantle viscosity from an inversion of the Fennoscandian relaxation data, *Geophys. J. Int, 114,* 45-62, 1993.

Moresi, L.-N., and V.S. Solomatov, Numerical investigations of 2D convection with extremely large viscosity variations, *Phys. Fluids, 7*, 2154-2162, 1995.

Nataf, H.-C., Mantle convection, plates, and hotspots, *Tectonophysics, 187*, 361-371, 1991.

Ogawa, M., G. Schubert, and A. Zebib, Numerical simulations of three-dimensional thermal convection in a fluid with strongly temperature dependent viscosity, *J. Fluid Mech., 233,* 299-328, 1991.

Olson, P., An experimental approach to thermal convection in a two-layered mantle, *J. Geophys. Res., 89,* 11293-11301, 1984.

Olson, P., G. Schubert, and C. Anderson, Plumes formation in the D" layer and the roughness of the core-mantle boundary, *Nature, 327*, 409-413, 1987.

Olson, P., G. Schubert, and C. Anderson, Structure of axisymmetric mantle plumes, *J. Geophys. Res., 98,* 6829-6844, 1993.

Osako, M., and E. Ito, Thermal diffusivity of $MgSiO_3$ perovskite, *Geophys. Res. Lett., 18,* 239-242, 1991.

Parmentier, E.M., C. Sotin, and B.J. Travis, Turbulent 3D thermal convection in an infinite Prandtl number, volumetrically heated fluid: Implications for mantle dynamics, *Geophys. J. Int., 116*, 241-251, 1994.

Patankar, S.V., *Numerical Heat Transfer and Fluid Flow*, Hemisphere, New York, 1980.

Pollack, H.N., S.J. Hurter, and J.R. Johnson, Heat flow from the Earth's interior—Analysis of the global data set, *Rev. Geophys., 31,* 267-280, 1993.

Press, W.H., S.A. Teulolsky, W.T. Vetterling, and B.P. Flanncry, *Numerical Recipes (2nd ed.)*, Cambridge Univ. Press, New York, 1992.

Rayleigh, Lord, On convective convective currents in a horizontal layer of fluid, when the higher temperature is on the under side, *Philos. Mag., Ser. VI, 32,* 529-546, 1916.

Ricard, Y., M. A. Richards, C. Lithgow-Bertelloni, and Y. LeStunff, A geodynamic model of mantle density heterogeneity, *J. Geophys. Res., 98,* 21,895-21,909, 1993.

Richter, F.M., Experiments on the stability of convection rolls in fluids whose viscosity depends on temperature, *J. Fluid Mech., 89,* 553-560, 1978.

Richter, F.M., H.C. Nataf, and S.F. Daly, Heat transfer and horizontally-averaged temperature of convection with large viscosity variations, *J. Fluid Mech., 129,* 173-192, 1983.

Schmeling, H., Compressible convection with constant and variable viscosity: The effect on slab formation, geoid, and topography, *J Geophys. Res., 94*, 12,463-12,481, 1989.

Schubert, G., Subsolidus convection in the mantles of terrestrial planets, *Annu. Rev. Earth Planet. Sci., 7*, 289-342, 1979.

Schubert, G., Numerical models of mantle convection, *Annu. Rev. Fluid. Mech., 24,* 359-394, 1992.

Schubert, G., and C.A. Anderson, Finite element calculations of very high Rayleigh number thermal convection, *Geophys. J. R. Astron. Soc., 80*, 575-601, 1985.

Schubert, G., D.J. Stevenson, and P. Cassen, Whole mantle cooling and the radiogenic heat source contents of the Earth and Moon, *J. Geophys. Res., 85*, 2531-2538, 1980.

Schubert, G., G.A. Glatzmaier, and B. Travis, Steady, three-dimensional, internally heated convection, *Phys. Fluids A, 5*, 1928-1932, 1993.

Sclater, J.G., C. Jaupart, and D. Galson, The heat flow through oceanic and continental crust and the heat loss of the Earth, *Rev. Geophys., 18*, 269-311, 1980.

Sharpe, H.N., and W.R. Peltier, Parameterized mantle convection and the Earth's thermal history, *Geophys. Res. Lett., 5,* 737-740, 1978.

Sleep, N.H., An analytic model for a mantle plume fed by a thermal boundary layer, *Geophys. J. R. Astron. Soc., 90*, 119-128, 1987.

Sleep, N.H., Hotspots and mantle plumes: Some phenomenology, *J Geophys. Res., 95*, 6715-6736, 1990.

Smolarkiewicz, P.K., A fully multidimensional positive definite advection transport algorithm with small implicit diffusion, *J Comput. Phys., 54*, 325-362, 1984.

Solomatov, V.S., Scaling of temperature dependent and stress-dependent viscosity convection, *Phys. Fluids, 7*, 266-274, 1995.

Solomon, S.C., S.E. Smrekar, D.L. Bindschadler, R.E. Grimm, W.M. Kaula, G.E. McGill, R.J. Phillips, R.S. Saunders, G. Schubert, S.W.

Squyres, E.R. Stofan, Venus Tectonics - an overview of Magellan observations, *J. Geophys. Res., 97*, 13199-13255, 1992.

Stacey, F.D., *Physics of the Earth, 3rd ed.*, 513 pp., Brookfield, Kenmore, Queensland, Australia, 1992.

Stocker, R.L., and M.F. Ashby, On the rheology of the upper mantle, *Rev. Geophys., 11,* 391-426, 1973.

Su, W.-J., R.L. Woodward, and A.M. Dziewonski, Degree-12 model of shear velocity heterogeneity in the mantle, *J. Geophys. Res., 99,* 6945-6980, 1994.

Tackley, P.J., Effects of strongly temperature dependent viscosity on time-dependent, three-dimensional models of mantle convection, *Geophys. Res. Lett., 20,* 2187-2190, 1993.

Tackley, P.J., Three-dimensional models of mantle convection: influence of phase transitions and temperature dependent viscosity, Ph.D. thesis, Calif. Inst. of Technol., Pasadena, 1994.

Tackley, P.J., D.J. Stevenson, G.A. Glatzmaier, and G. Schubert, Effects of an endothermic phase transition at 670 km depth in a spherical model of convection in the Earth's mantle, *Nature, 361,* 699-704, 1993.

Tackley, P.J., D.J. Stevenson, G.A. Glatzmaier, and G. Schubert, Effects of multiple phase transitions in a 3-D spherical model of convection in the Earth's mantle, *J. Geophys. Res., 99,* 15877-15901, 1994.

Torrance, K.E., and D.L. Turcotte, Thermal convection with large viscosity variations, *J. Fluid Mech., 47,* 113-125, 1971.

Tozer, D.C., The present thermal state of the terrestrial planets, *Phys. Earth Planet. Inter., 6,* 182-197, 1972.

Travis, B.J., P. Olson, and G. Schubert, The transition from two-dimensional to three-dimensional planforms in infinite-Prandtl-number thermal convection, *J. Fluid Mech., 216,* 71-91, 1990a.

Travis, B., S. Weinstein, and P. Olson, Three-dimensional convection planforms with internal heat generation, *Geophys. Res. Lett., 17,* 243-246, 1990b.

Turcotte, D.L., and G. Schubert, *Geodynamics: Applications of Continuum Physics to Geological Problems,* John Wiley, New York, 1982.

van Keken, P.E., D.A. Yuen, and A.P. van den Berg, Implications for mantle dynamics from the high melting point of perovskite, *Science, 264,* 1437-1439, 1994.

Weertman, J., The creep strength of the Earth's mantle, *Rev. Geophys. Space Phys., 8,* 146-168, 1970.

Weertman, J., and J.R. Weertman, High temperature creep of rock and mantle viscosity, *Annu. Rev. Earth Planet. Sci., 3,* 293-315, 1975.

Weinstein, S.A., and U. Christensen, Convection planforms in a fluid with a temperature dependent viscosity beneath a stress-free upper boundary, *Geophys. Res. Lett., 18,* 2035-2038, 1991.

Weinstein, S.A., and P. Olson, Planforms in thermal convection with internal heat sources at large Rayeigh and Prandtl numbers, *Geophys. Res. Lett., 17,* 239-242, 1990.

Weinstein, S.A., and P.L. Olson, Thermal convection with non-Newtonian plates, *Geophys. J. Int., 111,* 515-530, 1992.

White, D.B., The planforms and onset of convection with a temperature dependent viscosity, *J. Fluid Mech., 191,* 247-286, 1988.

Whitehead, J.A., and B. Parsons, Observations of convection at Rayleigh numbers up to 760,000 in a fluid with large Prandtl number, *Geophys. Astrophys. Fluid Dyn., 9,* 201-217, 1978.

Young, R.E., Finite-amplitude thermal convection in a spherical shell, *J. Fluid Mech, 63,* 695-721, 1974.

Yuen, D.A., and S. Zhang, Equation of state and rheology in deep mantle convection, in *Perovskite: A Structure of Great Interest to Geophysics and Materials Science, Geophys. Monogr., vol. 45,* edited by A. Navrotsky and D.J. Weidner, pp. 131-137, AGU, Washington, D.C., 1989.

Yuen, D.A., D.M. Reuteler, S. Balachandar, V. Steinbach, A.V. Malevsky, and J.J. Smedsmo, Various influences on 3-dimensional mantle convection with multiple phase transitions, *Phys. Earth Planet. Inter., 86,* 185-203, 1994.

P.J. Tackley, Department of Earth and Space Sciences, University of California, Los Angeles, CA 90095. (e-mail: ptackley@ess.ucla.edu)

(Received April 19, 1995; revised October 16, 1995;
accepted October 19, 1995.)